T H E U N I V E R S I T Y O F T U L S A

THE GRADUATE SCHOOL

A DATA-DRIVEN OPTIMAL PRODUCTION CONTROL STRATEGY FOR UNCONVENTIONAL RESERVOIRS

by
Yuchen Zhang

A thesis submitted in partial fulfillment of

the requirements for the degree of Master of Science

in the Discipline of Petroleum Engineering

The Graduate School

The University of Tulsa

2016

T H E U N I V E R S I T Y O F T U L S A

THE GRADUATE SCHOOL

A DATA-DRIVEN OPTIMAL PRODUCTION CONTROL STRATEGY FOR UNCONVENTIONAL RESERVOIRS

by
Yuchen Zhang

A THESIS

APPROVED FOR THE DISCIPLINE OF

PETROLEUM ENGINEERING

By Thesis Committee

_____, Chair
Rami M. Younis

_____
Mohan Kelkar

_____
Ram Mohan

ABSTRACT

Yuchen Zhang (Master of Science in Petroleum Engineering)

A Data-driven Optimal Production Control Strategy for Unconventional Reservoirs

Directed by Dr. Rami M. Younis

66 pp., Chapter 5: Conclusions and Recommendations

(373 words)

The economic effectiveness of petroleum reservoir development largely relies on a proper design of the well control strategy. However, decision-making for the bottom hole pressure (BHP) schedule is challenging due to the lack of accurate information about the geologic formation and fluid properties. Engineers have to resort to techniques such as well logging and well testing to obtain information about the subsurface reservoir. But these methods are usually very expensive and time-consuming.

The wellhead production data, however, already offers valuable information about the underground rock and fluid properties. The reservoir history matching utilizes the surface data to reduce the uncertainty of the model. Combined with production optimization, it becomes a powerful tool to assist in decision-making of reservoir management. Nevertheless, it could be challenging to choose an appropriate prior model when only a weak reservoir characterization is available. Even if a random model is selected and matches the data perfectly, it may still be far from the true model due to the non-uniqueness of the solutions to inverse problems and thus not be able to predict future production accurately.

An alternative data-driven algorithm is proposed in this work to enhance the production from fractured unconventional reservoirs where limited knowledge of the reservoir is available. Requiring nothing more than production data, the method provides an active control decision-making workflow that is easy to apply in practice. The wellbore pressure is constrained to drop or hold in order to test how the reservoir responds and a decision will be made for the next BHP control step based on the response of the current step. The reservoir surface response is determined by the interaction of underground static and dynamic variables. The core idea of the algorithm is that, instead of making an the effort to calibrate the static variables and then predict the interaction of the dynamic variable, the study focuses on correlating the surface response and the optimal BHP controls directly. An analysis is carried out to explain this correlation in detail.

The proposed method is compared with optimization solutions and a naïve solution. It is proven that the data-driven method performs similarly to computational optimization solutions that assume complete knowledge of the system. Moreover, it is demonstrated that naïve control strategies can lead to non-optimal results.

ACKNOWLEDGEMENTS

The two-year experience at The University of Tulsa is full of happiness and challenges. First, I would like to express my gratitude to my academic advisor, Rami Younis, who made this journey possible. Dr. Younis is a visionary scholar as well as an easy-going friend. He never had a problem offering encouragement and support when I was frustrated. I would also like to extend my sincere thanks to Dr. Mohan Kelkar and Dr. Ram Mohan for being on my thesis committee and offering valuable comments on the thesis.

I gratefully acknowledge the financial support of the Cimarex. My sincere thanks go to Dr. Leslie Thompson for providing inspiration, ideas and valuable feedback from industry.

I am fortunate to have had the company of many friends who have brought me happiness during the two years. Especially, I would like to thank my colleague Zhe Liu for bringing a sense of humor to the office. I also would like to thank my housemates, Guotong Ren and Yu Zhao, who had made a desirable living environment.

Last but not least, I thank my parents, my grandma, my aunt and uncle who offer their understanding and unconditional love to me. I also would to like express my thank to my lifelong friends, Xue Liu, Shaobo Hua, Jingdo Guo and Shi Han, who have been patient listeners and understood my ambition.

TABLE OF CONTENTS

LIST OF FIGURES

LIST OF TABLES

CHAPTER 1

INTRODUCTION

The production decision-making of reservoir management relies on the prediction power of a reliable reservoir model. This model can be a physics-based mechanistic model such as a 3D multi-phase model or a simplified 1D radial proxy. A physics-based model is more interpretable, but it requires accurate characterization of the reservoir to improve its prediction power. A complete characterization should involve knowledge of not only reservoir engineering but also petrophysics, geology, geomechanics, geophysics, and etc. However, such a comprehensive model is usually not available at the early stages of reservoir development. From the perspective of a reservoir engineer, an initial reservoir model should be established based on the direct measurement data and can be iteratively improved through inference techniques which make use of history data.

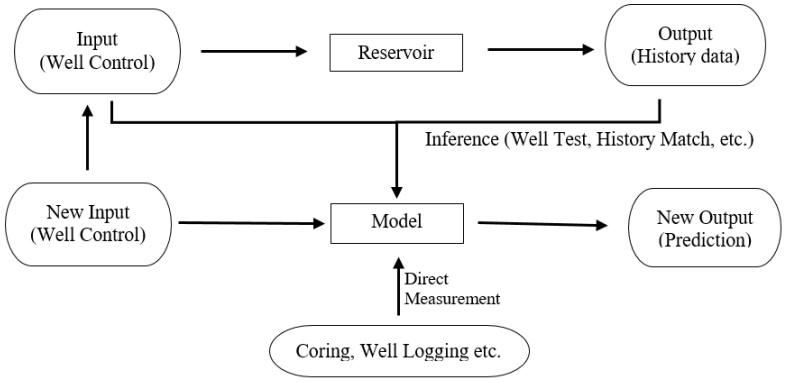

Figure 1.1 Flow Chart on How A Reservoir Model is Built and Improved

Most of the strategy making tools like model-based optimization heavily rely upon a well-characterized reservoir model which is not always accessible. In this study, a data-

driven algorithm is proposed to improve the production from fractured unconventional reservoirs where very limited information about the geologic formation and fluid properties are available a priori. Rather than making significant efforts to build an explicit comprehensive model, the proposed method takes advantage of the specific surface response patterns of the fractured reservoir and correlates them with the best production strategies.

The method offers an active control decision-making workflow that is easy to apply in practice. Through synthetic test cases, the proposed method is proven to perform comparably to computational optimization solutions that assume complete knowledge of the system. Moreover, it is demonstrated that naïve control strategies can lead to solutions which are far from the optimal results.

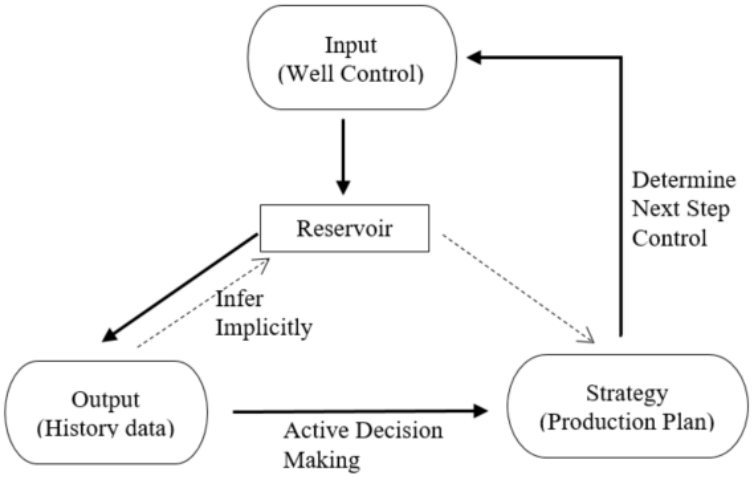

Figure 1.2 Info Flow Chart of the Proposed Data-Driven Algorithm

1.1 Literature Review

Computational production optimization, also known as model-based optimization, is a powerful tool to develop an improved operating plan for a particular reservoir of

interest. The algorithm approaches the optimal solution by searching the high-dimensional variable space. Because the optimization involves the prediction of future production, it requires a reservoir simulation model to serve as the estimator of the objective function (usually, it is the life-cycle net present value (NPV)). Optimization algorithms can be divided into two categories: derivative-free methods and gradient-based methods. An important distinction is between the methods that attempt to find the global optimum and those that aim at finding a local optimum (Jansen, 2009). A naïve optimization method relies on a single model to make decisions. The inaccuracy of such model would significantly undermine the performance of the optimization.

One of the greatest challenges of the model-based optimization is making decisions in the presence of large uncertainties about the subsurface structure and the parameters that influence the production (Jansen, 2009). There are three major ways to deal with the uncertainty: robust optimization, multi-objective optimization, and closed-loop optimization. Jansen et al. (2005) were among the first to utilize the robust optimization for generating the optimal production plans. A set of plausible geological models (also known as ensembles of geological realizations) is considered to represent the uncertainty. The expectation of the NPVs over a set of possible reservoir realizations is regarded as the objective function. Based on the concept of robust optimization, Liu and Reynolds (2015) provided a multi-objective optimization algorithm to maximize the expectation of NPVs and minimize the risk simultaneously. Specific methods applied include the classical weighted sum method and the normal boundary intersection method. Chen (2009) and Jansen (2009) proposed a closed-loop optimization framework. In their work, they introduced a system consisting of two parts: geological model updating and robust

production optimization. The optimization process follows an iterative workflow where the geological model is updated continuously to be consistent with the production data through the data assimilation process, and an optimized strategy is chosen based on the updated model.

Although various ways have been tried to cope with the uncertainty of geology and fluid properties, the model-based optimization still suffers from two drawbacks. First, the closed-loop optimization requires a well-built initial reservoir model to serve as the starting point of the optimization procedure. In reality, people will not always have sufficient prior knowledge to build such a model. Second, it is difficult to obtain a suitable production strategy at the beginning stage of the production because the early decision is made based on a rough initial model.

When the acquisition of a sufficient data set is not financially feasible, data-driven methods which only require production data have became promising alternatives for the model-based optimization. Gupta (2014) applied data mining and time series analysis to forecast production in shale reservoirs of the Barnett, Bakken and Eagle Ford plays. A neural network model is built and trained on the history data of the previous year and subsequently used to predict future performance. The author found that the quality of prediction is highly dependent on the input data quality. Noisy and inconsistent input leads to unreliable predictions. Schuetter (2015) implemented both simple linear regression and advanced methods such as Random Forest, Support Vector Machine, Gradient Boosting and Multi-dimensional Kriging to analyze the performance of a reservoir from the Wolfcamp shale formation in the Permian Basin. Data including well location, well completion time, azimuth angle, etc. were considered to be the features of the training

model. Details about how to train and tune the statistical models were also discussed in their work. The statistical learning algorithms are finally used to identify factors that separate good wells from poor performers.

The data-driven models mentioned above can run much more quickly than a physics-based reservoir simulation model because they are just mathematical proxies of real reservoirs. A major problem of the data-driven models is that human efforts are required to select, train and tune a suitable mathematical model for a particular reservoir. This process can be very tedious which involves the selection of features and the regularization. If an overcomplicated design is selected, a large amount of data is required to overcome the high variance. On the other hand, if the model is too simple to represent the true reservoir, it will suffer from large bias (Hastie, 2001). A second drawback of applying statistical methosd on reservoir performance prediction and optimization is that statistical methods are usually not as interpretable as physics-based models. This research, however, will propose a 'data-driven' method that is intuitive and fully interpretable which could serve as an alternative for model-based optimization.

1.2 Concepts and Conventions

Wellhead oil-gas ratio (OGR) is the primary indicator applied in the data-driven algorithm for decision-making. OGR is used here instead of more commonly used gas-oil ratio (GOR) because it is more intuitive and easier to explain in the context of the algorithm. Given a bottom hole pressure (BHP) schedule, the increase or decrease in OGR is referred to as OGR response. Such response provides significant information about reservoir fluid properties. The OGR response per unit time is defined as response rate.

In the context of this thesis, the naïve strategy refers to a schedule that keeps dropping the BHP at the maximum rate from the beginning of the production and then maintain producing at the lowest wellbore pressure allowed. For simplicity, the naïve approach is labeled ‘Strategy 1’. The well control plan generated by the optimization algorithm is referred to as ‘Strategy 2’ and the data-driven solution is ‘Strategy 3’.

The metric applied to evaluate the performance of a well control plan is the five-year NPV. A better solution is indicated by a larger five-year NPV. Within the scope of this thesis, the NPV is computed with 45$/bbl oil price, 2.2$/MMBtu gas price, and 12% cash depreciation rate.

1.3 Layout of the Thesis

There are five chapters and one appendix in this thesis. In Chapter 2, an investigation of the underlying physics behind the reservoir OGR response patterns is presented. It is shown that the relative permeability curve is the most important influence factor to the OGR response. Chapter 3 introduces the computational optimization algorithm, and related topics on the stochastic gradient, line search strategy, etc. are discussed. The optimal BHP schedules for test cases are also presented and compared with the naïve approach to explore the reservoir potential for optimization. By the end of this chapter, two important conclusions are made. First, holding BHP or slowing down the drop rate at the early production stage will yield a positive OGR response which would benefit the long-term NPV. Second, for reservoirs with S-shape fractional flow curves, the improvement could be obtained from optimization is limited. In Chapter 4, a data-driven algorithm is proposed based on the surface OGR response discussed in Chapter 2. The

method is proved to perform comparably to the computational optimization algorithm introduced in Chapter 3. Chapter 5 presents the conclusions and a brief discussion of the challenges and suggestions for practical application. Finally, the detailed parameter set-up of the reservoir simulation model is given in Appendix A.

CHAPTER 2

SIMULATION STUDY ON RESERVOIR RESPONSE

An underground reservoir can be considered to be a black box. Given an input, the reservoir responds with an output. The input is a set of controls or constraints that operators exert on wells which penetrate the reservoir. For example, the producers or injectors can be operated under a specific rate or bottom hole pressure. The output is a series of quantitative values that change over time, such as oil production rate, bottom hole pressure, total oil production and water cut. In this work, the output is also referred to as reservoir response. The study of the reservoir response helps us better understand what is inside the 'black box' and make a wiser decision based on the knowledge.

The reservoir simulator is a powerful tool to evaluate and explore the potential of oil and gas reservoir. Modern reservoir engineering techniques like automatic history matching and production optimization highly rely on reservoir simulation studies. For this research, a reservoir simulation model is built to represent the true reservoir and its output is studied. The simulation tool will also be utilized to explore the underground state variables and their relationship with the surface response. The reservoir simulation model in this chapter is built and implemented through the Schlumberger Eclipse E100 commercial simulator. In Section 2.3, a simulator based on the Automatically Differentiable Expression Templates Library (ADETL) framework (Younis 2011) will be used together with E100 to validate an underground saturation build up phenomenon.

2.1 Reservoir Model

This section will introduce the simulation set-up for the study including gridding, PVT model, and relative permeability model. The relative permeability plays a significant role in this research. Several types of relative permeability curves are generated to cover the complexity and uncertainty of real reservoirs.

2.1.1 Gridding and Formation Properties

A reservoir simulation model with a multi-stage fractured well is built. A real fractured well has 20 fracturing stages and 4 fractures for each stage. So ultimately, 80 fractures intersect with the horizontal wellbore. The reservoir model established represents one-fourth of the real fractured well with 40 half fractures intersecting with the horizontal wellbore. Log local grid refinement is applied to the grids around the fractures and wellbore to make more accurate predictions.

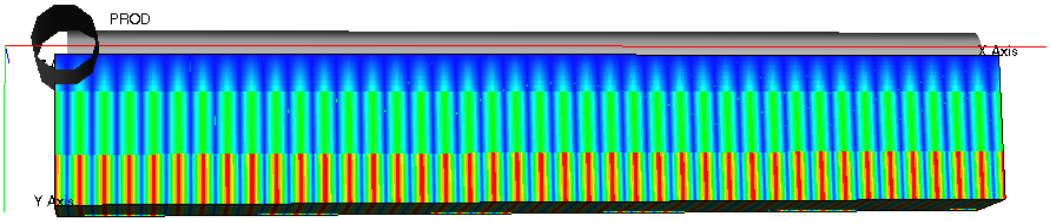

Figure 2.1 Reservoir Model

Refer to the table 6.1 in Appendix A for more reservoir properties.

2.1.2 PVT Data

The oil and gas PVT data is shown in the figures and tables below; the bubble point is set to be 5000 psi.

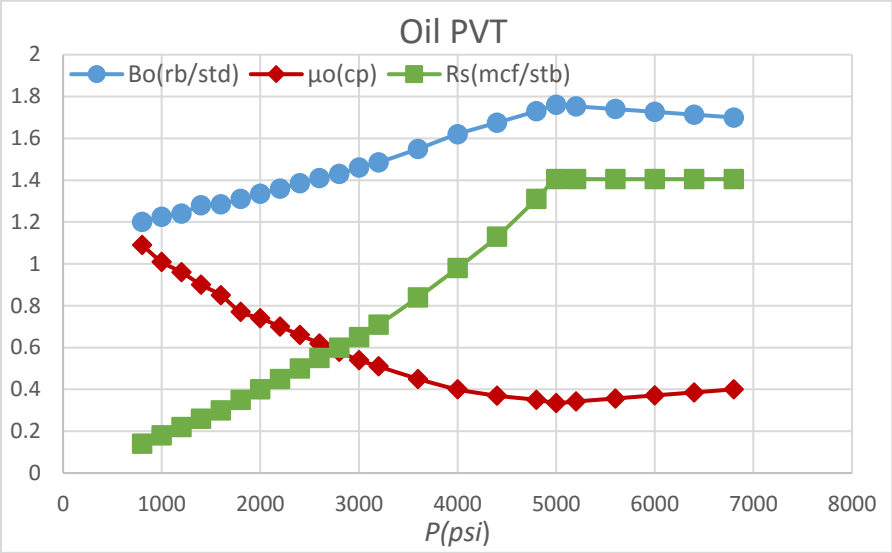

Figure 2.2 Oil PVT

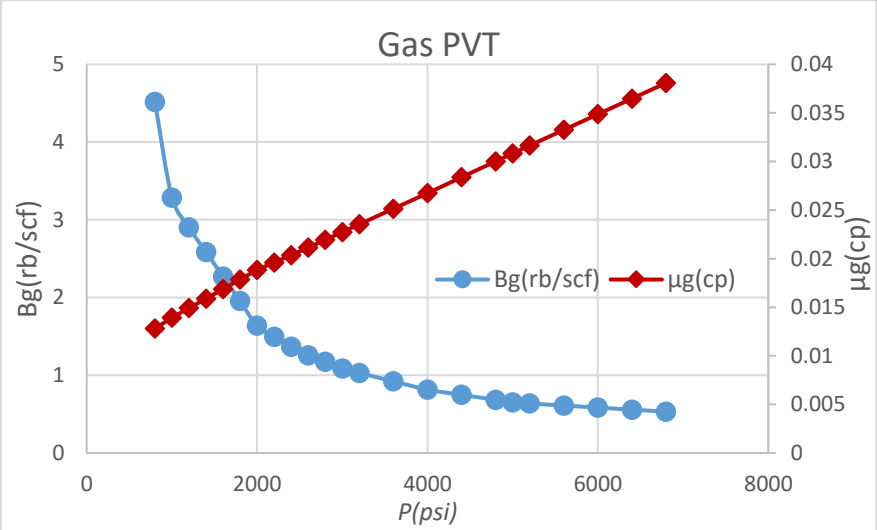

Figure 2.3 Gas PVT

2.1.3 Relative Permeability Model

Four sets of relative permeability curves are generated by implementing Corey's model and used to test the algorithm. Corey's model is characterized by the equations below:

$$k_{ro} = K_{ro,max}\left(\frac{S_o - S_{or}}{1 - S_{or} - S_{gc}}\right)^{n_o}, \qquad 2.1$$
$$k_{rg} = K_{rg,max}\left(\frac{S_g - S_{gc}}{1 - S_{or} - S_{gc}}\right)^{n_g},$$

where S_{or} and S_{gc} denote residual oil saturation and critical gas saturation; $K_{ro,max}$ and $K_{rg,max}$ represent maximum oil relative permeability and gas relative permeability; n_o and n_g are exponents which range from 1 to 6. The exponents determine the curvature of the permeability functions of each phase. Larger exponents mean more concave permeability curves and is more sensitive to S_o when S_o is close to 1.

The oil flow fraction function, which is of more importance to the study, can be derived once the relative permeability and viscosity of oil and gas phases are known. The relation is given by,

$$f_o = \frac{1}{1 + \frac{k_{rg} k_{ro}}{\mu_o \mu_g}}. \qquad 2.2$$

The equation neglects gravity and capillary pressure. While k_{rg} and k_{ro} are treated as functions of saturation, S_o, μ_o and μ_g are functions of and pressure, P. The study assumes $\mu_o = 0.45\ cp$ and $\mu_g = 0.0268\ cp$ to make the factional flow curves below (Figure 2.4), but in reality, viscosity will actually change with the pressure and the simulation process will capture this dynamic change. The constant viscosity setting here is for visualization.

In this study, S_{or} and S_{gc} are set to be 0.2 and 0, oil exponential term n_o will take a value of 2 and gas exponential term n_g is set to be 0.5, 1, 2 and 4 to make fractional flow curves with various shapes.

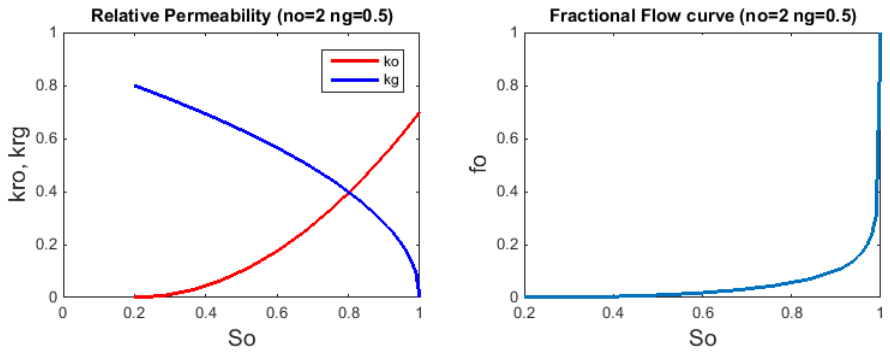

(a) ng = 0.5

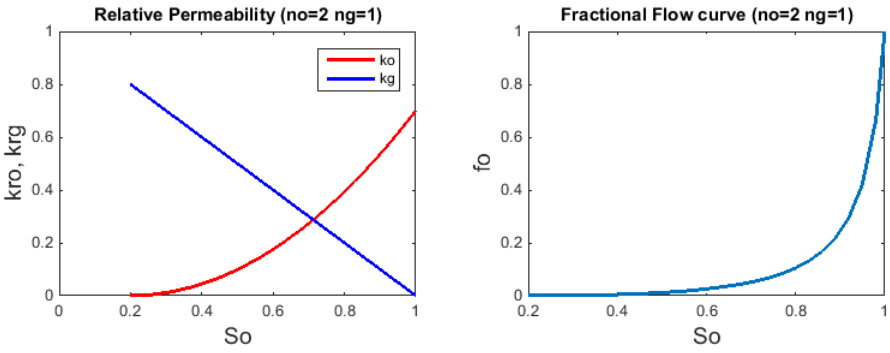

(b) ng = 1

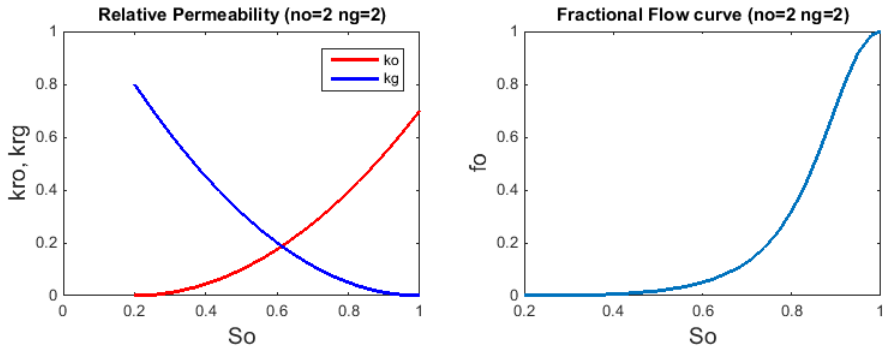

(c) ng = 2

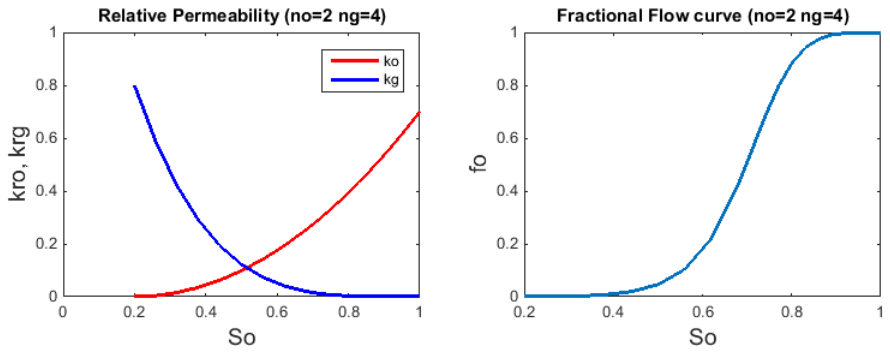

(d) ng = 4

Figure 2.4 Relative Permeability Curves and Fractional Flow Curves

2.2 Reservoir Surface Response

The reservoir model described in Section 2.1 can be considered to be a black box. A proper input is given, and output is obtained. Here, the input is the BHP control schedule, and the output can be any response that is generated throughout the reservoir simulation life, for example, the cumulative oil production or reservoir pressure. In this study, wellhead oil-gas ratio (OGR) is considered as an output. With the help of simulation tools, the study investiages how the OGR responds to the various BHP schedules. The response patterns are discussed in detail along with two major insights the OGR provides. Afterward, the underground saturation and pressure, which are considered as outputs, will also be investigated.

2.2.1 Reservoir Response When Dropping Pressure

In this section, tests are made to explore how the reservoir responds when BHP drops from above to below the bubble point pressure, P_b. Starting from the initial reservoir pressure (6000 psi), the well bottom hole pressure is reduced to 1000 psi within 62.5 days (with 80 psi/day). Note that the BHP will drop to P_b = 5000 psi within 12.5 days. Figure 2.5 shows the surface OGR response of 4 cases with different relative permeability curves (Section 2.1.3).

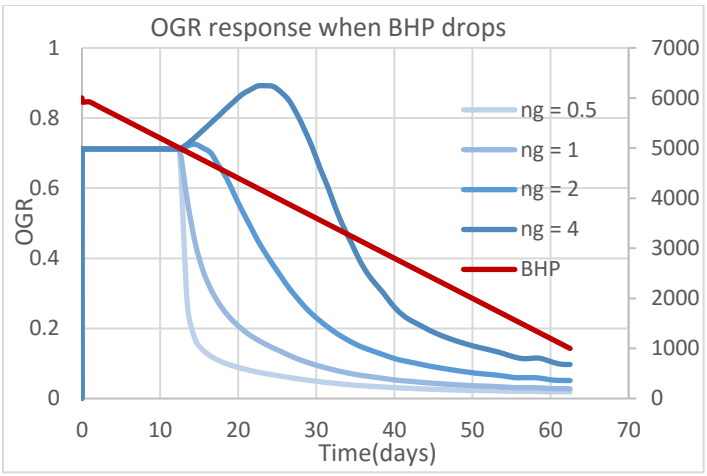

Figure 2.5 Reservoir Surface Response When Pressure Drops

Results show that different relative permeability inputs lead to distinct responses. Above the bubble point pressure, the OGR remains constant for all cases. Below the P_b, the OGR drops directly for the *ng = 0.5* and *ng = 1* cases, while for S-shape fractional flow curve cases (*ng = 2* and *ng = 4*) the OGR tends to build up before decreasing.

The observation above proves that pressure drop test below bubble point pressure is an effective way to distinguish differences among all relative permeability curves. Further analysis on the surface OGR responses will be shown in later sections.

2.2.2 Reservoir Response When Holding Pressure

A study is made by holding the wellbore pressure constant after a steep drop. The BHP is controlled to decrease from 6000 psi to 4600 psi within 17.5 days and then maintained at 4600 psi. Figure 2.6 displays the BHP change versus time and the surface OGR responses.

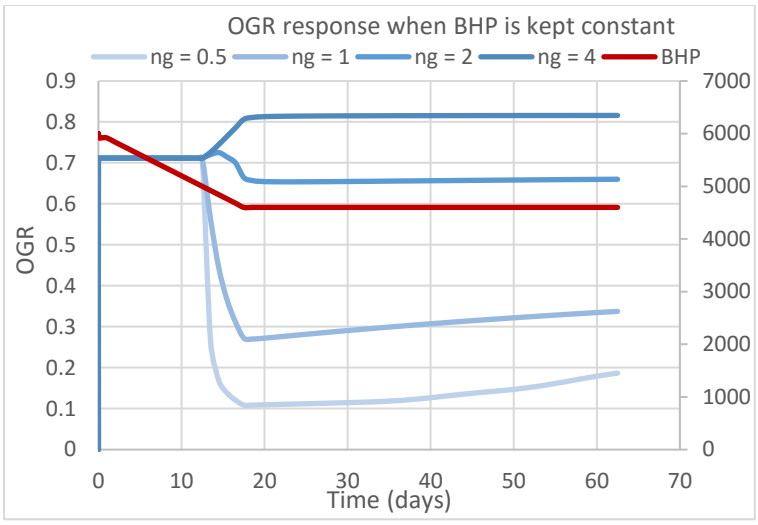

Figure 2.6 Reservoir Surface Response When Pressure Drops and Holds

Different types of relative permeability yield four different OGR responses. The OGR goes up then down (as shown in Figure 2.6) and remains constant once the pressure is held for the *ng = 2* and *ng = 4* cases. However, for *ng = 0.5* and *ng = 1* cases, the OGR goes down and has a tendency to rebound when pressure is maintained. The observations about the surface OGR responses are of great importance for the design of a data-driven well-control algorithm. The next section will discuss the inner mechanism of the reservoir response in detail.

2.3 Underground Response

The reservoir surface response provides significant information for well-control decision-making. This section discusses why the reservoir responds the way as presented in Section 2.2 by exploring the connection between the surface OGR response and underground saturation variation. It was found that the OGR is positively related to the saturation. A detailed qualitative analysis was made to clarify this connection. Additionally, a simple one-dimension model was built to investigate the underground saturation build-

up phenomenon. This phenomenon was observed and confirmed by multiple simulation trials with both the Eclipse E100 and the ADETL simulator. Morever, a one-cell analysis was carried out trying to explain the fluid mechanism behind the phenomenon.

2.3.1 Connection Between OGR and Underground Variables

The surface response should be a function of the underground response. It is essential to study and understand the connection between the surface and underground response. This work specifically focuses on the study of the relationship between the surface production OGR and the underground state variables (pressure and oil saturation). This relation is represented by the equation below,

$$OGR = \frac{V_{o,std}}{V_{g,std}} = \frac{(q_{o,r}/B_o)\cdot t}{(q_{o,r}R_s/B_o + q_{g,r}/B_g)\cdot t}, \tag{2.3}$$

$$OGR = \frac{1}{178R_s + \frac{B_o}{5.615B_g}\frac{1-f_o}{f_o}}. \tag{2.4}$$

In the equation, 178 comes from the unit conversion of R_s from mcf/stb to rb/stb and 5.615 comes from the conversion of B_g from rb/scf to rb/stb. Note that the viscosity (μ), solution oil gas ratio (R_s), oil formation volume factor (B_o), and gas formation volume factor (B_g) are all functions of pressure while the oil flow fraction (f_o) is a function of saturation. Accordingly, the OGR can be written as a function of oil pressure (P) and saturation (S_o) at the wellbore (or at the fracture).

$$OGR = F(P, S_o). \tag{2.5}$$

How the OGR relates to P depends on the PVT properties and how it relates to S_o is partially determined by PVT (see 2.2) and partially depends on relative permeabilities.

Ignoring the minor effect of viscosity (μ), OGR versus S_o relation should solely depend on relative permeabilities.

To understand how surface responses change with time, we can take the derivative to time for 2.4,

$$\frac{\partial OGR}{\partial t} = \left(\frac{\partial OGR}{\partial R_s}\frac{\partial R_s}{\partial P} + \frac{\partial OGR}{\partial \left(\frac{B_o}{B_g}\right)}\frac{\partial \left(\frac{B_o}{B_g}\right)}{\partial P}\right)\frac{\partial P}{\partial t} + \frac{\partial OGR}{\partial f_o}\frac{\partial f_o}{\partial S_o}\frac{\partial S_o}{\partial t}, \quad 2.6$$

and then simplify the equation above,

$$\frac{\partial OGR}{\partial t} = C_p\frac{\partial P}{\partial t} + C_s\frac{\partial S_o}{\partial t}, \quad 2.7$$

where,

$$C_p = \frac{\partial OGR}{\partial R_s}\frac{\partial R_s}{\partial P} + \frac{\partial OGR}{\partial \left(\frac{B_o}{B_g}\right)}\frac{\partial \left(\frac{B_o}{B_g}\right)}{\partial P}, \quad 2.8$$

$$C_s = \frac{\partial OGR}{\partial f_o}\frac{\partial f_o}{\partial S_o}. \quad 2.9$$

C_p denotes the pressure contribution rate. It represents the influence on the OGR per unit pressure change. Similarly, C_s is the contribution to the OGR per unit saturation change. The two contribution rates along with the absolute change of pressure and saturation determine how the surface OGR responds.

To further simplify the analysis, we can take the derivative on $R_s, B_o/B_g$ and f_o for 2.4. Because the R_s, $\frac{B_o}{B_g}$, and f_o are always greater than 0, the following equations can be derived,

$$\frac{\partial OGR}{\partial R_s} = -\left(178R_s + \frac{B_o(1-f_o)}{5.615B_g f_o}\right)^{-2} 178 < 0, \quad 2.10$$

$$\frac{\partial OGR}{\partial (B_o/B_g)} = -\left(178R_s + \frac{B_o(1-f_o)}{5.615B_g f_o}\right)^{-2}\frac{1-f_o}{5.615f_o} < 0, \quad 2.11$$

$$\frac{\partial OGR}{\partial f_o} = (178R_s + \frac{B_o(1-f_o)}{5.615B_g f_o})^{-2} \frac{B_o}{5.615B_g} \frac{1}{{f_o}^2} > 0. \quad 2.12$$

It is now known that the OGR is negatively correlated to R_s and $\frac{B_o}{B_g}$, and positively correlated to f_o. Relative magnitudes of the derivatives are determined by 178, $\frac{1}{5.615f_o}$ and $\frac{B_o}{5.615B_g{f_o}^2}$. Furthermore, when it is below the bubble point R_s and $\frac{B_o}{B_g}$ are both monotonic increasing w.r.t pressure P (Figure 2.2 and Figure 2.7). f_o considered here is also a monotonic increasing function of S_o as was discussed in Section 2.1.3. That is to say,

$$\frac{dR_s}{dP} > 0, \text{ for } P < P_b, \quad 2.13$$

$$\frac{d(B_o/B_g)}{dP} > 0, \text{ for } P < P_b, \quad 2.14$$

$$\frac{df_o}{dS_o} > 0, \text{ for all } S_o \in [0,1]. \quad 2.15$$

From 2.8-2.15, it is obvious that C_p<0 and $C_s > 0$. This implies the negative correlation between the OGR and pressure and the positive correlation between the OGR and saturation.

For now, S_o is treated as an independent variable and the contributions to the surface response from S_o and P are considered separately. However, under certain circumstance, S_o can be assumed as a dependent on pressure P. They are nonlinearly correlated and $\frac{\partial S_o}{\partial P}$ tends to be greater than 0 when the pressure change rate is large.

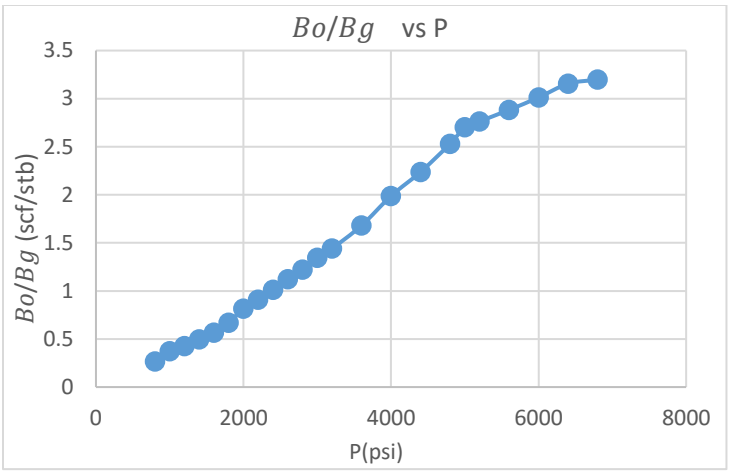

Figure 2.7 Bo/Bg vs P Plot

The following analysis explains the OGR versus pressure or OGR versus saturation correlations for each well-control stage more concretely.

Firstly, when the BHP is above the bubble point pressure (P_b), no gas comes out from the oil liquid. S_o remains to be 1 and R_s, B_o, B_g, μ are almost constant over the pressure (Figure 2.2 and Figure 2.3). Thus, the OGR remains constant.

Secondly, when pressure drops under the bubble point pressure (P_b), $\frac{\partial P}{\partial t} < 0$. The change of the OGR is governed by two factors: the decline in pressure which positively contributes to the OGR and the decrease in saturation which has a negative influence. The surface OGR response depends on the interaction of both factors. At this pressure control stage, the assumption that S_o is a dependent of P is reasonable although strictly S_o should be a function of both wellbore pressure P and time t. However, when the decline rate of BHP is large, t has little influence on saturation and the OGR can be treated as a function of P. Application of the S_o- P dependency assumption to 2.7 gives,

$$\frac{\partial OGR}{\partial t} = C_p \frac{\partial P}{\partial t} + C_s \frac{\partial S_o}{\partial P} \frac{\partial P}{\partial t}, \qquad 2.16$$

where $C_p = \frac{\partial OGR}{\partial R_s}\frac{dR_s}{dP} + \frac{\partial OGR}{\partial (B_o/B_g)}\frac{d(B_o/B_g)}{dP}$, $C_s = \frac{\partial OGR}{\partial f_o}\frac{\partial f_o}{\partial S_o}$. According to Figure 2.2 and Figure 2.7, $\frac{dR_s}{dP}$ and $\frac{d(B_o/B_g)}{dP}$ are almost constant when the pressure is below bubble point. For convenience, $\frac{dR_s}{dP}$ will be denoted by c_1 and $\frac{d(B_o/B_g)}{dP}$ will be denoted by c_2. Substituting 2.10-2.12 into the formula of C_p and C_s yields,

$$C_p = -178c_1\left(178R_s + \frac{B_o(1-f_o)}{5.615B_g f_o}\right)^{-2} - \frac{c_2(1-f_o)}{f_o}\left(178R_s + \frac{B_o(1-f_o)}{5.615B_g f_o}\right)^{-2}, \quad 2.17$$

$$C_s = \frac{B_o}{5.615B_g}\frac{1}{{f_o}^2}\left(178R_s + \frac{B_o(1-f_o)}{5.615B_g f_o}\right)^{-2}\frac{\partial f_o}{\partial S_o}. \quad 2.18$$

Substituting the above equations into 2.16, we obtain

$$\frac{\partial OGR}{\partial t} = \frac{\partial P}{\partial t}\left(178R_s + \frac{B_o(1-f_o)}{5.615B_g f_o}\right)^{-2}\left(\frac{B_o}{5.615B_g}\frac{1}{{f_o}^2}\frac{\partial f_o}{\partial S_o}\frac{\partial S_o}{\partial P} - 178c_1 - \frac{c_2(1-f_o)}{f_o}\right). \quad 2.19$$

Replace the always-positive term $\left(178R_s + \frac{B_o}{5.615B_g f_o}\right)^{-2}$ by symbol *D*, we obtain

$$\frac{\partial OGR}{\partial t} = D\frac{\partial P}{\partial t}\left(\frac{B_o}{5.615B_g}\frac{1}{{f_o}^2}\frac{\partial f_o}{\partial S_o}\frac{\partial S_o}{\partial P} - 178c_1 - \frac{c_2(1-f_o)}{f_o}\right). \quad 2.20$$

$\frac{B_o}{5.615B_g}\frac{1}{{f_o}^2}\frac{\partial f_o}{\partial S_o}\frac{\partial S_o}{\partial P}$ is regarded as the contribution of saturation while $-(178c_1 + \frac{c_2(1-f_o)}{f_o})$ is the influence of pressure. $\frac{\partial P}{\partial t}$ is negative and the sign of the above equation is determined by the difference of $\frac{B_o}{5.615B_g}\frac{1}{{f_o}^2}\frac{\partial f_o}{\partial S_o}\frac{\partial S_o}{\partial P}$ and $178c_1 + \frac{c_2(1-f_o)}{f_o}$; The OGR increases if $178c_1 + \frac{c_2(1-f_o)}{f_o} > \frac{B_o}{5.615B_g}\frac{1}{{f_o}^2}\frac{\partial f_o}{\partial S_o}\frac{\partial S_o}{\partial P}$

From the slope of oil PVT curve (Figure 2.2 Oil PVT), c_1 is around 3×10^{-4} and c_2 is around 1.5×10^{-4}. $\frac{\partial f_o}{\partial S_o}\frac{\partial S_o}{\partial P}$ is important to determine the sign of $\frac{\partial OGR}{\partial t}$ if f_o is not extremely close to zero. The study of Section 2.3 will focus on the two derivatives.

$\frac{\partial f_o}{\partial S_o}$ is the slope of the oil-gas fractional flow curve which is pre-determined by the properties of the reservoir fluid. Generally, when the slope is large, the OGR tends to decrease with time and vice versa. In another way, if f_o is a weak function of S_o the positive influence triggered by the decrease in pressure will be overwhelming compared with the negative contribution by the reduction in saturation and the $\frac{\partial OGR}{\partial t}$ will be larger than 0. On the opposite, saturation contribution will dominate when f_o is very sensitive to S_o.

Finally, when wellbore pressure is kept, R_s, B_o and B_g can all be treated as constants and, the OGR is determined solely by S_o. Now, S_o is a function of time only. With the monotonic fractional flow curve, the OGR positively correlates to S_o. Therefore, for pressure holding period, it is reasonable to simply study the change of underground oil saturation,

$$OGR = F(S_o(t)), \tag{2.21}$$

$$\frac{\partial OGR}{\partial t} = \frac{\partial OGR}{\partial S_o}\frac{\partial S_o}{\partial \mathrm{t}} = \frac{\partial OGR}{\partial f_o}\frac{\partial f_o}{\partial S_o}\frac{\partial S_o}{\partial \mathrm{t}}. \tag{2.22}$$

Substituting 2.12 into 2.22, yields,

$$\frac{\partial OGR}{\partial t} = \left(178R_s + \frac{B_o(1-f_o)}{5.615B_g f_o}\right)^{-2}\frac{B_o}{5.615B_g}\frac{1}{{f_o}^2}\frac{\partial f_o}{\partial S_o}\frac{\partial S_o}{\partial \mathrm{t}}. \tag{2.23}$$

Since $\frac{\partial OGR}{\partial f_o} > 0$ (2.12) and f_o is a monotonic increasing function of t, the sign of $\frac{\partial OGR}{\partial t}$ is determined by the derivative of saturation with respect to time. The magnitude of

$\frac{\partial OGR}{\partial t}$ depends on the absolute value of f_o, the steepness of fractional flow curve ($\frac{\partial f_o}{\partial S_o}$), and the saturation change with time ($\frac{\partial S_o}{\partial t}$). In Section 2.3.2, the study will focus on $\frac{\partial f_o}{\partial S_o}$ and $\frac{\partial S_o}{\partial t}$.

In summary, above the bubble point, the OGR barely changes. When the pressure drops below the bubble point pressure, the OGR fluctuation is the result of a combination of pressure and saturation contributions. Specifically, the OGR is affected by f_o, the derivative of the S_o-f_o function and the nonlinear relation between P and S_o (2.20). When the pressure holds below the bubble point, S_o-f_o function is the dominant factor that governs the intensity of OGR response. It is also necessary to study the saturation-vs-time relation at this stage (2.23).

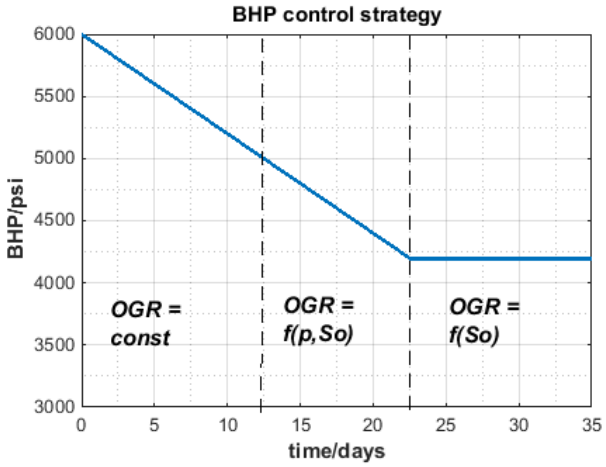

Figure 2.8 The Relation Between OGR and Underground State Variables for Each Well Control Stage

2.3.2 Underground Saturation change

A pressure drop-and-hold test was made to test the reservoir subsurface response (oil saturation change). According to the simulation results, oil saturation decreases simultaneously with the pressure as the BHP drops below bubble point. This observation

validates the previous assumption (2.16) that saturation S_o is positively correlated with wellbore pressure P ($\frac{\partial S_o}{\partial P} > 0$) when the pressure drops fast. Additionally, when the pressure suddenly holds, the saturation of the underground fracture and blocks around the fracture will increase.

To illustrate the reservoir reaction, a one-dimension simplified model was built which has only one fracture. The space between each fraction is 50 ft. The 1D model represents the right half of the fracture space which should be 25 ft wide (Figure 2.9). There are 250 grid blocks in this model, and the dimension of each grid block is 0.1ft×50ft×200ft. The drop-and-hold test applied four relative permeability curves which were described in Section 2.1.3. Other reservoir properties are the same as the original model. The leftmost block represents the fracture and characterizes the effect of well sink with the Peaceman Method. The following figure illustrates how this one-dimension model is built.

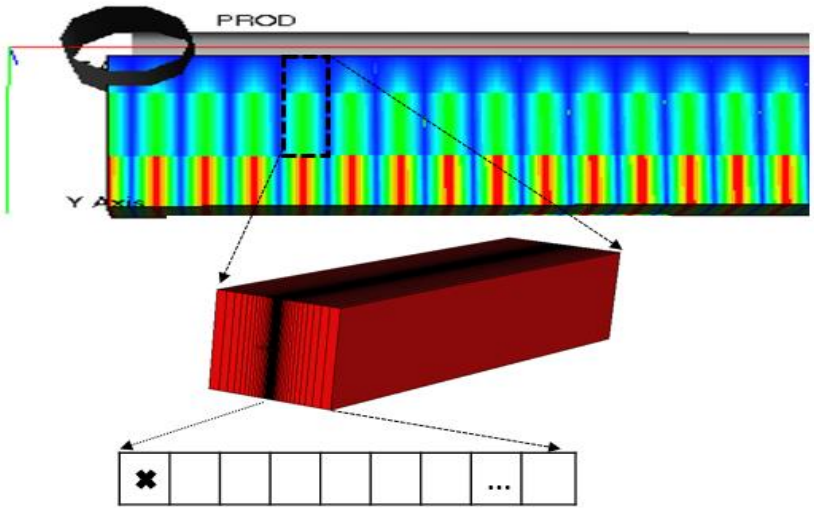

Figure 2.9 Sketch of Simplified 1D Model

A simulation was run that the BHP drops from 6000 psi to 4000 psi in 25 days and then suddenly holds. The oil saturation of fracture block (the leftmost cell) versus time is

presented in Figure 2.10. Notice that as the pressure drops below bubble point pressure (5000 psi), the S_o begins to go down. Once we start to keep the pressure constant, S_o builds up.

Let's focus on the pressure dropping period first. Below the P_b, while S_o falls concurrently with P for all cases, $\frac{\partial S_o}{\partial P}$ is larger for cases with steeper fractional flow curves (ng=0.5 and ng=1). Steeper curve implies that gas gains more mobility with the same amount of pressure decreases. As gas is easier to escape to the wellhead, it takes up pore volume less efficiently, and saturation drops relatively slow.

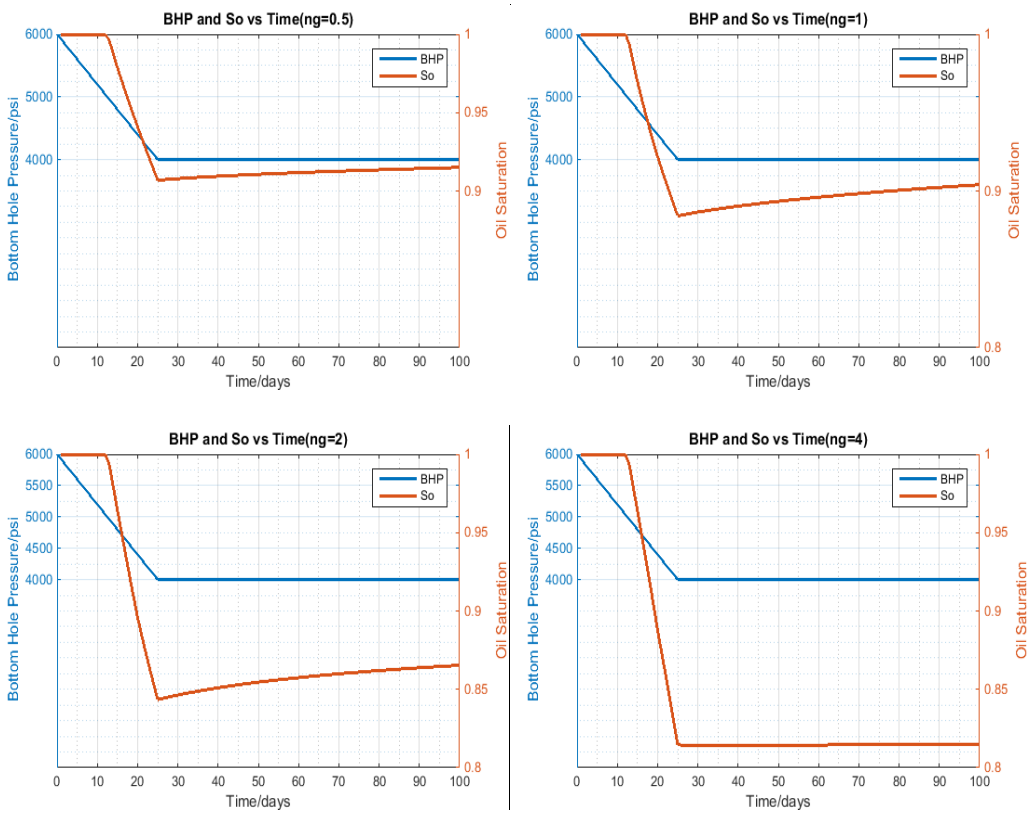

Figure 2.10 BHP and Saturation Response for Different Cases

Denote $\frac{\partial P}{\partial t}$ by a negative constant value $-c$ and subsititute it into 2.19, we obtain,

$$\frac{\partial OGR}{\partial t} = cD(178c_1 + \frac{c_2(1-f_o)}{f_o} - \frac{B_o}{5.615B_g}\frac{1}{{f_o}^2}\frac{\partial f_o}{\partial S_o}\frac{\partial S_o}{\partial P}). \quad 2.24$$

From the above equation, $\frac{\partial S_o}{\partial P}$ contributes negatively to the OGR. However, the influence of $\frac{\partial S_o}{\partial P}$ is limited compared with the contribution of as $\frac{\partial f_o}{\partial S_o}$. Over different cases, $\frac{\partial S_o}{\partial P}$ is positive and differs twice at most, while $\frac{\partial f_o}{\partial S_o}$ ranging from approximately 0 (ng=4 case) to 50 (ng=0.5 case) makes much bigger differences. The cases with S-shape fractional curves (*ng = 2* and *ng = 4* cases) have larger $\frac{\partial S_o}{\partial P}$ and smaller $\frac{\partial f_o}{\partial S_o}$ while the cases with steep monotonic fractional flow curves (*ng = 0.5* and *ng = 1* cases) are the opposite. Now, it is easy to understand the surface OGR response pattern in Figure 2.5, $\frac{\partial OGR}{\partial t}$ is greater than zero when BHP drops just below the bubble point for *ng = 4* and *ng = 2* case since $\frac{\partial f_o}{\partial S_o}$ is almost 0 when S_o is close to 1 (Figure 2.4). The pressure contribution overwhelms the saturation contribution leading to a positive OGR response. On the contrary, for the *ng = 0.5* and *ng = 1* case, the negative contribution from saturation is dominant and the OGR response is negative because $\frac{\partial f_o}{\partial S_o}$ is relatively large.

Based on the simulation results, when the pressure is held, the oil saturation of the perforated block and bottom hole oil flow fraction will build up, therefore returning the positive OGR response. However, how the reservoir will respond is determined by the relative permeability of oil and gas. Specifically, the response rate is positively correlated to the slope of fraction flow curve (see 2.23). For example, given the following relative permeability curve (*ng = 0.5*) and fractional flow curve, we can divide the curve into a strong response saturation part and a weak response part.

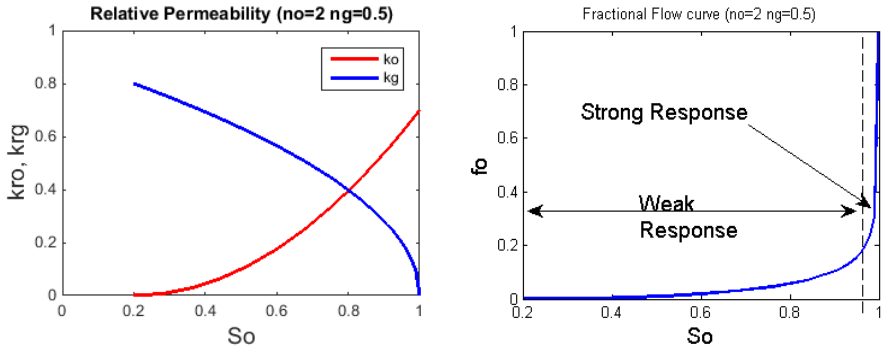

Figure 2.11 Response Zone for ng=0.5 case

Bottom-hole saturation holds back slightly as the BHP holds. If the saturation is greater than 0.9, the slight increase in S_o yields a significant increase in f_o and turns out a strong OGR response, while if the S_o is within the weak response region, a negligible OGR increase is expected.

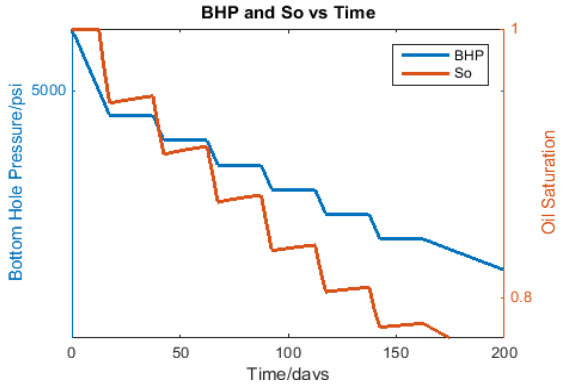

Figure 2.12 BHP and Saturation Response Under Drop-Hold=Drop Test For Case ng=1

To further explore the saturation build-up phenomenon, another test was made on the *ng = 1* case, that the bottom hole pressure was set to drop and keep alternatively. This drop-hold-drop schedule displays a clearer pattern that oil saturation will build up every time the BHP starts to be held constant after a dramatic drop.

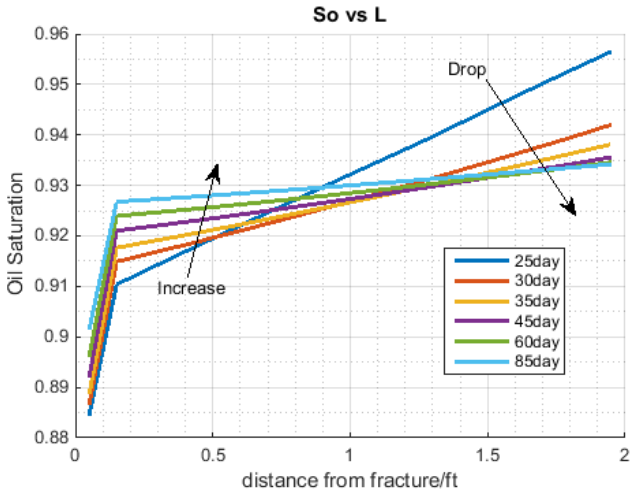

Figure 2.13 Oil Saturation Profile When Pressure Holds for ng = 1 case – The Simulation Result Given by Eclipse E100 (Note that the BHP starts to be kept at 25th day)

However, from the oil saturation profile (Figure 2.13) it is evident that the saturation build-up only happens within a small proximity to the fracture. Oil saturation of cells far away from the fracture will decrease. In another word, the gas will move backward into the reservoir.

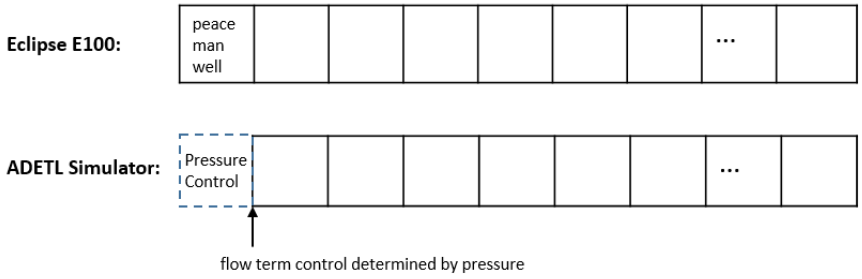

Figure 2.14 Comparison of Eclipse E100 1D Model and ADETL 1D Model

Besides the Eclipse 1D model illustrated above, another pressure boundary model is built as a validation. As shown in Figure 2.14, the model has 249 grid blocks plus a ‘ghost block’ on the leftmost. The ‘ghost block’ is the fracture and the model treats the fracture pressure as the bottom hole pressure. In this case, the BHP is set to drop first and then held constant. As the pressure of the fracture was controlled, the flux flows through

the face of the 'ghost block' and the first real block can be determined. Note that this pressure boundary model is closer to a real situation in that the fracture is assumed to be an infinite conductivity flow channel with zero pressure gradient while the fracture in the Peaceman Well Model is a real grid block with a pressure gradient.

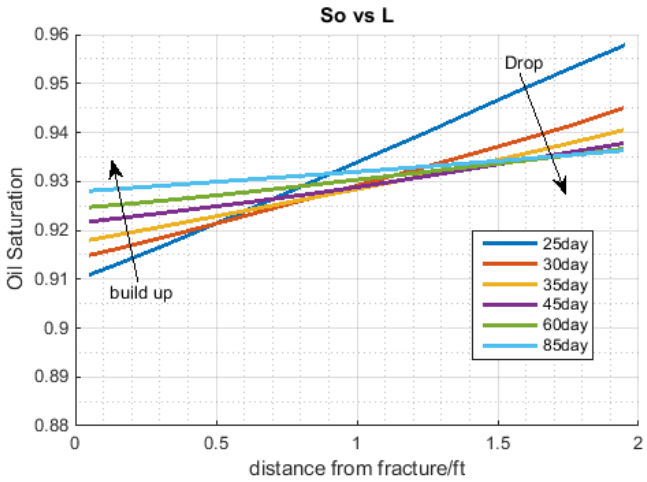

Figure 2.15 Oil Saturation Profile When Pressure Holds for *ng = 1* case – The Simulation Result Given by ADETL Simulator (Note that pressure starts to be kept at 25th day)

The saturation profile shows the same trend as it is in the Eclipse simulation result. There is no saturation gap between the first and second grid block as it was in Figure 2.13. This is because the fracture cell does not exist in the simulation model. The leftmost cell represents the first non-fracture block.

The saturation build up seem to be counterintuitive, but the material balance of a single cell can explain the dynamic.

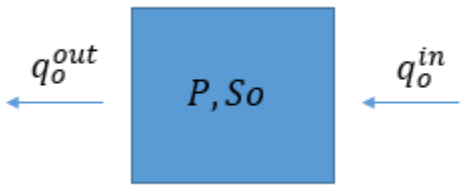

Figure 2.16 Sketch of One-cell Model

Consider the material balance equation of one cell,

$$\frac{\emptyset_2 VSo_2}{Bo_2} - \frac{\emptyset_1 VSo_1}{Bo_1} = \Delta t[q_{o\,std}^{in} - q_{o\,std}^{out}]. \quad 2.25$$

Note that the q_o^{in} and q_o^{out} in this equation are surface flow rate. If we assume minor effect of rock and fluid compressibility ($\emptyset$, B_o), the equation would be,

$$So_2 - So_1 = \frac{1}{\emptyset V}\Delta t[q_{o\,r}^{in} - q_{o\,r}^{out}]. \quad 2.26$$

After simplification, we obtain,

$$\frac{dS}{dt} = \frac{1}{\emptyset V}[f_o^{in} q_{t\,r}^{in} - f_o^{out} q_{t\,r}^{out}], \quad 2.27$$

where, f_o^{in}, f_o^{out} are determined by So, $q_{t\,r}^{in}$, $q_{t\,r}^{out}$ are determined by Pressure gradient.

From 2.27, it is evident that if $f_o^{in} q_{t\,r}^{in} > f_o^{out} q_{t\,r}^{out}$ the oil saturation of the single cell will build up, otherwise, it will fall. On one hand, in the figure of P_o, S_o profile and the figure of f_o and pressure gradient (dP_o) at day 30 (Figure 2.17), the pressure gradient is almost constant for the grids close to fracture. The f_o, however, increase monotonically with the distance. This indicates that if we consider any small block within this scope, we will have $f_o^{in} q_{t\,r}^{in} > f_o^{out} q_{t\,r}^{out}$ and consequently S_o will increase with time according to 2.27. Note that the scope of the constant dP_o consists with the pressure build up area observed from Figure 2.13 and Figure 2.15.

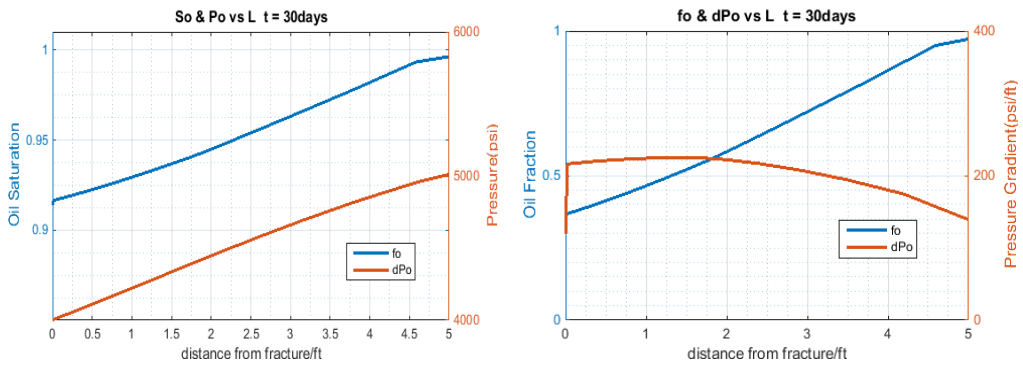

(a) (b)

Figure 2.17 Oil Saturation and Pressure Profile along with Oil Flow Fraction and Pressure Gradient Profile at Day 30 (When the Pressure Holds)

On the other hand, for day 22 which is before the pressure hold, dP_o is no longer constant and $f_o^{in} q_{tr}^{in} > f_o^{out} q_{tr}^{out}$ is not guaranteed any more and S_o in the fracture grid keeps dropping on day 22 (Figure 2.18).

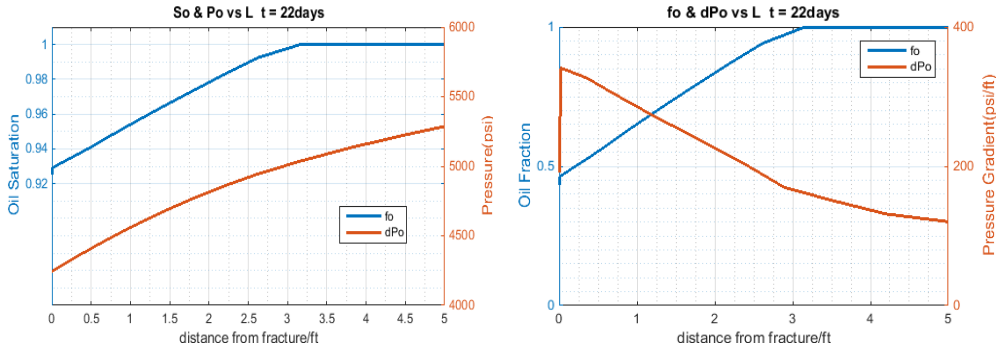

(a) (b)

Figure 2.18 Oil Saturation and Pressure Profile along with Oil Flow Fraction and Pressure Gradient Profile at Day 22 (When the Pressure Drops)

In conclusion, when BHP declines below bubble point pressure, saturation decreases simultaneously. The variation of pressure contribution is negligible compared to the saturation's positive influence. $\frac{\partial f_o}{\partial S_o}$,however, is a major factor that determines the saturation contribution and consequently decides the sign of $\frac{\partial OGR}{\partial t}$. When BHP is then kept

constant, saturation builds up within a small proximity to the fracture. The influence power of this saturation surge on the OGR highly depends on the value of $\frac{\partial f_o}{\partial S_o}$.

In a word, $\frac{\partial f_o}{\partial S_o}$ is the most important factor that determines the sign and intensity of the OGR. In turn, the information of OGR response which reflects the relative magnitude of $\frac{\partial f_o}{\partial S_o}$ can be utilized to infer reservoir fluid properties.

CHAPTER 3

OPTIMIZATION ALGORITHM AND COMPARISON

Production optimization offers a powerful way to assist the design of well control or well placement strategies. If a true reservoir description is available, computer optimization program will lead to the global optimal or at least a local optimal solution. The study takes advantage of the optimization results in two ways. First, optimization solution is compared with a simple reference strategy (Strategy 1) to explore the reservoir potential for improvement. Second, optimization solution (Strategy 2) serves as a reference strategy to test the performance of the data-driven method which will be introduced later.

3.1 Solution by the Optimization Method

3.1.1 Optimization Algorithm Description

In order to validate the proposed algorithm, a numerical production optimization algorithm was implemented to obtain the optimal solution and to treat it as a reference well control strategy. Five-year NPV is set to be the objective to maximize, and it is treated to be a multi-variable function. The well BHPs at each time step are the independent variables. The numerical simulator serves as the evaluator of the NPV and the formula is shown below.

$$\max_{u} f(u) = NPV, \tag{3.1}$$

$$NPV = \sum_{n=1}^{N_t} \frac{r_o^n Q_o^n + r_g^n Q_g^n}{(1+b)^{t_n/365}}, \quad 3.2$$

where r_o^n and r_g^n denote oil and gas price respectively; N_t is the number of time steps; Q_o^n and Q_g^n represent the total oil and gas production of *nth* time step.

Essentially, the optimization procedure is to search for a combination of BHP controls that yields an "optimum" NPV. This searching process relies on the steepest descent algorithm with backtracking scheme. Other methods, such as conjugate gradient and quasi-Newton BFGS might be a more efficient way to capture an optimal solution if the exact gradient of the objective function is available. Nevertheless, to attain this gradient, the 'adjoint' matrix needs to be computed which requires the access to the simulator code, and this is not possible to obtain with a commercial reservoir simulator. Instead, the true gradient can be approximated by a stochastic gradient which only requires multiple evaluations of the NPV.

The following equation presents the basic formula of the steepest descent method.

$$x^{k+1} = x^k + \alpha_k \frac{d_k}{\|d_k\|_\infty}, \quad 3.3$$

where d_k is the search direction, and in this case it is the approximated gradient of the NPV $d_k = \nabla \hat{f}$; x is the variable space to be searched; x^k is the variable vector for kth search step; α_k is the line search step size for kth step.

In this problem, the naïve backtracking is applied. The step size α_k is chosen by a heuristic scheme. As a search direction is determined, the line search method starts from an initial α_k^0 and tries to update the variable vector by this α. If this vector does not return a better NPV, the algorithm cuts the step by half and repeat the same process. Otherwise, the algorithm accepts the step size α and corresponding NPV. If no NPV is accepted within

five cuts, the algorithm regenerates the search direction d_k.by resampling ensembles. The specific workflow is shown below,

Optimization Algorithm

- Set maximum step cut time N_{sc} = 5; set maximum resample time N_s =5; set initial step size $\alpha_0 = 0.1$; set maximum step size $\alpha_{max} = 0.1$.
- Calculate a search direction d_k
- Get new well control vector by search on d_k,
    1) $l = 0; is = 0;$
    2) $x_{k+1}^{trial} = x_k + \alpha_k \frac{d_k}{\|d_k\|}$;
    3) If $f(x_{k+1}^{trial}) > f(x_k)$ accept $x_{k+1} = x_{k+1}^{trial}$, $\alpha_{k+1}^0 = \min(2 * \alpha_k^l, \alpha_{max})$, $l = 0; is = 0;$
    Else,
        If $l > N_{sc}\ and\ is > N_s$, terminate the algorithm
        If $l \geq N_{sc}\ and\ is \leq N_s$, resample Ne ensembles, generate a new direction $d_k = d_k^{new}$, $l = 0, is++$ and return to 2)
        if $l \leq N_{sc}$, $\alpha_k = \frac{\alpha_k}{2}$, $l++$, return to 2)
        End If
    End If

The steepest descent method is sensitive to the scaling of the problem. Highly skewed variable space leads to an inefficient search path and extra steps. Therefore, scaling is applied to normalize and map every element in the variable space onto the [0,1] interval by $\tilde{x}_i = \frac{x_i - x_i^{\text{low}}}{(x_i^{\text{up}} - x_i^{\text{low}})}$ where $0 \leq \tilde{x}_i \leq 1$. x_i^{low} is the lower bound of the independent variable. In the context of the research, it is 1000 psi (P_{low}). x_i^{up} is the upper bound. In this study, it is 6000 psi (P_i).

Regarding stochastic gradient, an ensemble-based method was applied. The following is the gradient equation:

$$\nabla \hat{f} = \frac{1}{N_e - 1} C_x \sum_{j=1}^{N_e} \left(\hat{x}^j - \overline{\hat{x}}\right)\left(f\left(\hat{x}^j\right) - \overline{f}\right) \qquad 3.4$$

$$= \frac{1}{N_e - 1} C_x \cdot \Delta\hat{X} \cdot \Delta\hat{F}^T,$$

where $\overline{\hat{x}}$ is the sample mean (the average of the N_e samples); $f(\hat{x}^j)$ represents the evaluation of the objective function. In this case, it means to run the simulator once and evaluate five-year NPV; $\overline{f}$ is the average of the N_e NPV values, namely, $\frac{1}{Ne} * \sum_{j=1}^{N_e} f(\hat{x}^j)$, and $\Delta\hat{F}$ is illustrated by the equation below.

$$\begin{aligned} \Delta\hat{F} &= [\delta\hat{f}^1, \delta\hat{f}^2, \delta\hat{f}^3, \dots, \delta\hat{f}^{Ne}] \\ &= [f(\hat{x}^1) - \overline{f}, f(\hat{x}^j) - \overline{f}, \dots, f(\hat{x}^j) - \overline{f}]. \end{aligned} \quad 3.5$$

3.1.2 Optimization Solution and Comparison with Strategy One

Strategy 1 is a "naïve" production control plan that keeps dropping BHP from the beginning of the development as was introduced in Section 1.2. In this case, the Strategy 1 schedules the bottom hole pressure to drop from 6000 psi to 1000 psi with 80 psi per day. Consequently, it will take approximately two months before the wellbore pressure reaches 1000 psi.

Strategy 1 provides a reference solution and offers us the underlying potential of the reservoir. Comparison of the optimized schedule (Strategy 2) with the Strategy 1 provides the possibility of determining whether there is space to optimize for a particular reservoir or determining how much more NPV can be obtained if the optimized schedule is implemented. Figure 3.1 (a) presents the well BHPs of the two solutions and Figure 3.1 (b) compares the NPV. The yellow line in the plots represents the Strategy 1, while the red curve is the BHP and NPV for Strategy 2. An analysis based on OGR response was carried out as an explanation of the optimized well control pattern.

ng = 0.5

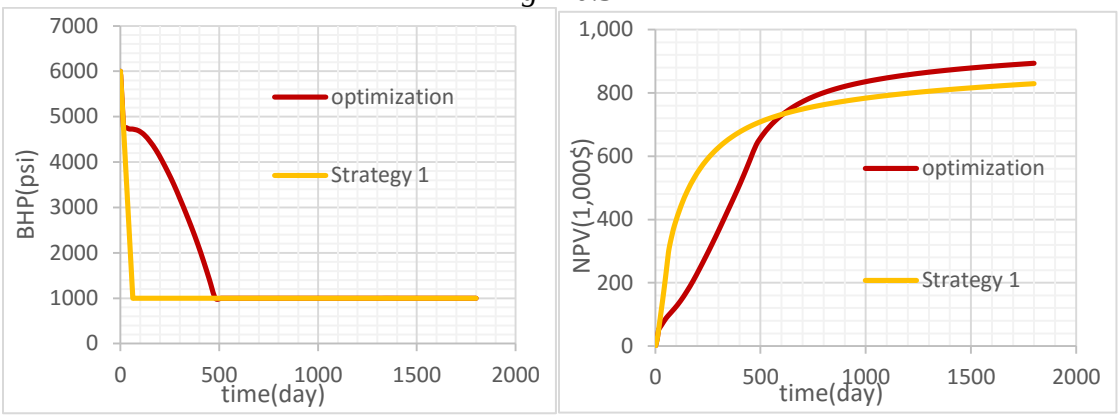

(a) (b)

Figure 3.1 Comparison of Strategy 1 and Strategy 2 for *ng = 0.5*

For the *ng = 0.5* case, the Strategy 2 started by quickly dropping the BHP, but suddenly the pressure was held at approximately 4800 psi and this hold period lasted about 100 days (the pressure dropped very slowly during the 100 days). The BHP then started to fall again at an increasing rate and finally reached 1000 psi at the 480th day. The pressure control curve ended up with a convex shape.

This pressure control pattern can be explained by partitioning the fractional flow curve into a strong and a weak OGR response parts. As was described in Section 2.3.2, $\frac{\partial f_o}{\partial S_o}$ determine the intensity of the OGR response. The BHP should be monitored to decrease in a very small rate while the reservoir is within the strong response region because of the large slope of S_o-f_o curve (Figure 3.2). Otherwise a dramatic pressure drawdown would reduce the proportion of oil produced. Because the strong response region of this type of reservoir is very narrow (Figure 3.2), the oil saturation quickly "passed through" the strong part into a weak response region where dropping the pressure quickly becomes the best strategy.

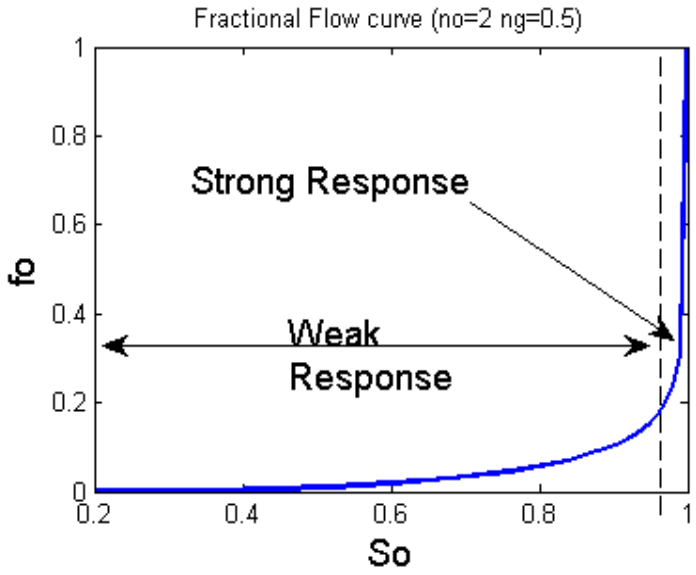

Figure 3.2 Fractional Flow Curve and Response Zone for *ng = 0.5*

ng = 1

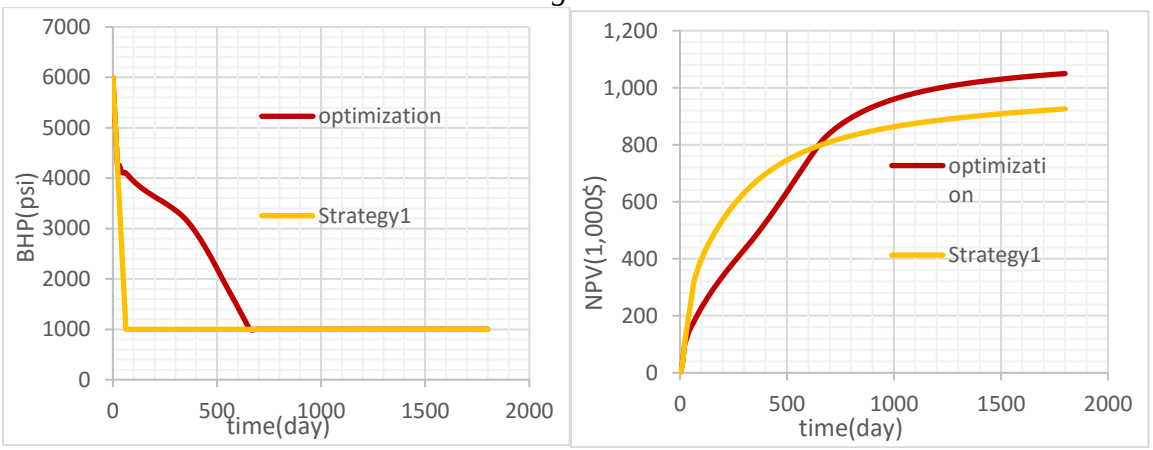

(a) (b)

Figure 3.3 Comparison of Strategy 1 and Strategy 2 for *ng = 1*

Like the *ng = 0.5* case, the well control solution of the *ng* = 1 case had a hold period (from the 30th day to the 360th day) and a sharp decreasing period (from the 360th day to the 660th day). Nevertheless, fractional flow curve of the *ng = 1* case is less steep but has a wider strong response region (Figure 3.4) which implies less negative effects for pressure dropping within strong response region. Thus, the pressure decline rate within the hold

period was not as slow as it was for the case with *ng = 0.5*. However, the hold time, on the contrary, lasted longer.

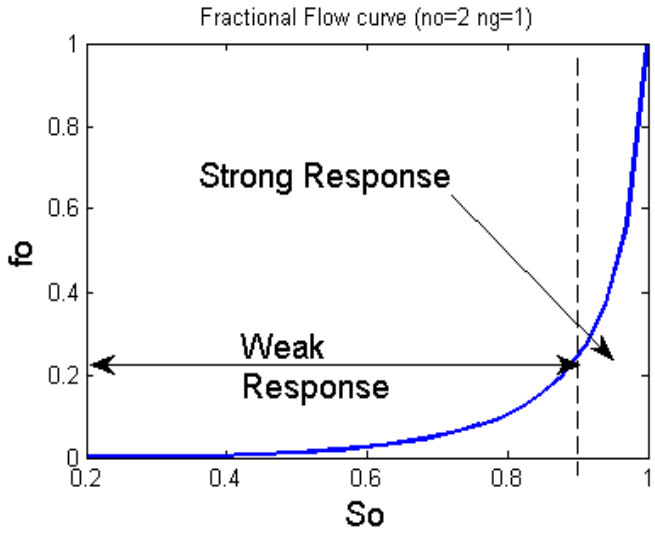

Figure 3.4 Fractional Flow Curve and Response Zone for *ng = 1*

ng = 2

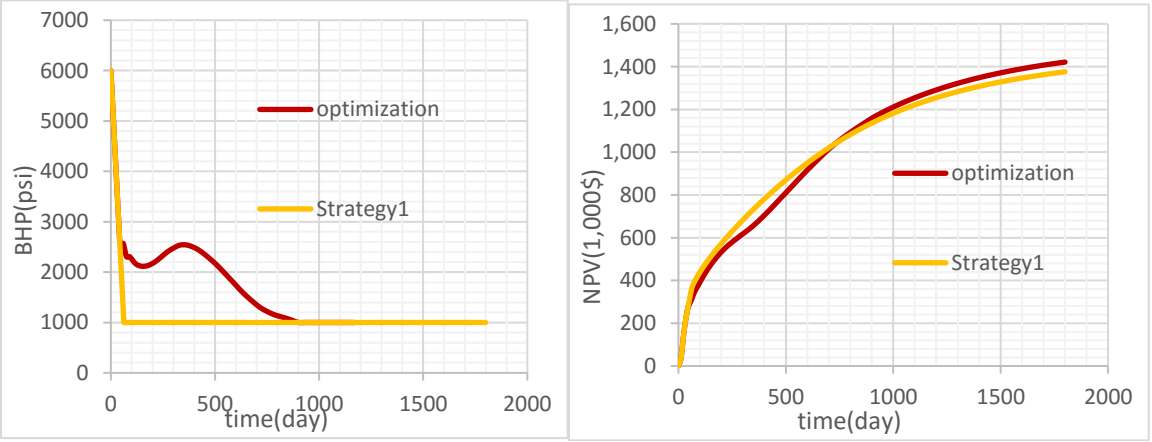

(a) (b)

Figure 3.5 Comparison of Strategy 1 and Strategy 2 for *ng = 2*

Unlike the previous two cases, the fractional flow curve of the *ng = 2* reservoir is not concave and has a flat region at the rightmost part of the curve (Figure 3.6). The shape of the curve is an "S". In other words, the second derivative of the curve is not monotonic. This new type of curve, especially its rightmost, part will significantly influence the production control strategy.

Compared with the former cases, Strategy 2 dropped the BHP much lower before the first pressure held at about 2500 psi. This control pattern indicates that the algorithm chooses to let the reservoir "skip" the rightmost weak response region. A second difference from former cases is that the "hold period" is not distinctly separated from other control periods. A reasonable explanation is that the fractional flow curve has a smoother shape than other cases so that there is no clear-cut distinction between the strong response region and the weak response part.

Another important aspect is that, in terms of 5-year NPV, the optimized solution is only improved slightly compared to Strategy 1. The reason is that the slope of the *ng = 2* curve is not steep enough, at least not as steep as previous fractional flow curves. That means the strong response region of this case is not "strong" enough. Therefore, relatively weaker OGR response is expected when the pressure holds, and less increase of oil proportion is expected from the wellhead.

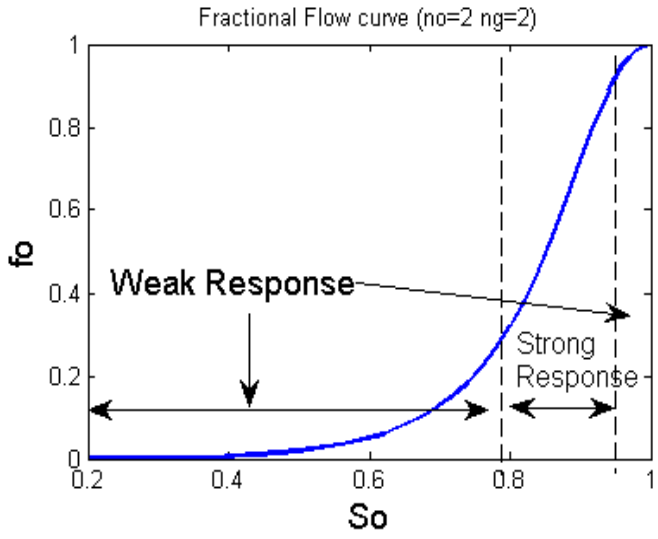

Figure 3.6 Fractional Flow Curve and Response Zone for *ng = 2*

ng = 4

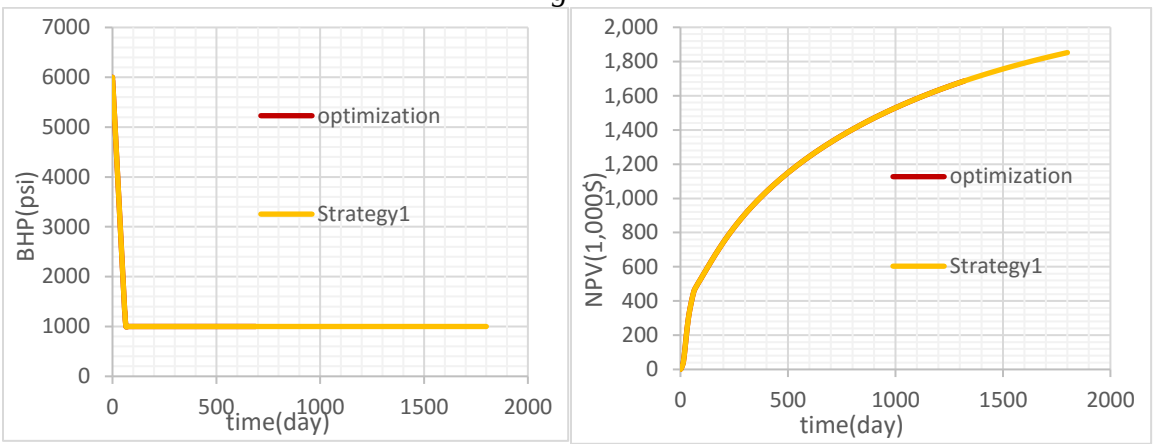

(a) (b)

Figure 3.7 Comparison of Strategy 1 and Strategy 2 for *ng = 4*

As for the *ng = 4* case, the optimized BHP control almost overlaps with the Strategy 1 which implies that there was little space to optimize the well control. Note that the rightmost flat zone is relatively wide for this case (Figure 3.8). Because the reservoir was not able to pass through this range before the BHP reaches 1000 psi, there was no need to hold the pressure.

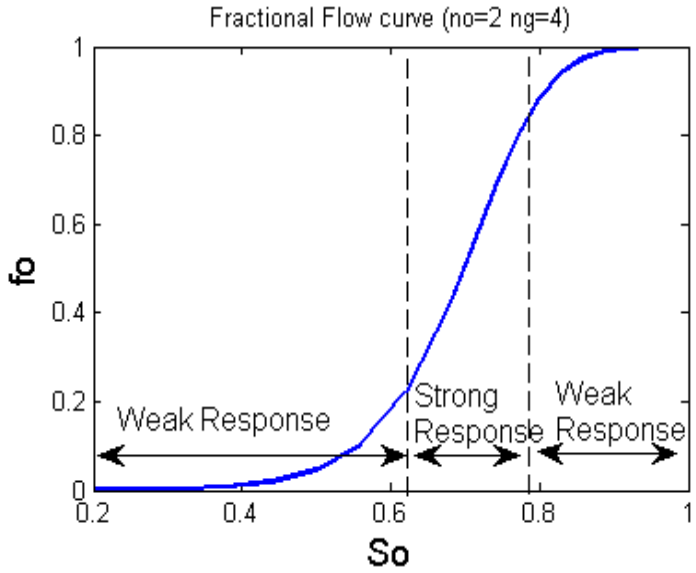

Figure 3.8 Fractional Flow Curve and Response Zone for *ng = 4*

Based on the analysis above, holding BHP or slowing down the drop rate at an early production stage will inspire a positive OGR response, which would benefit the long-term NPV. Furthermore, it is reasonable to conclude that the optimal BHP control mostly depends on the characteristic of relative permeability, i.e., the particular shape of the fractional flow curve. When the fractional flow curve is concave, optimization solution may give a considerable improvement on NPV. The pressure hold timing and duration depend on the width and steepness of the strong response part of the fractional flow curves. For a reservoir with an 'S-shape' fractional flow curve, optimized well schedule may not able to show a significant advantage over the naïve BHP control. A conservative and risk-free strategy for such reservoirs is to apply naïve control plan.

CHAPTER 4

DATA-DRIVEN WELL CONTROL ALGORITHM

The reservoir development decision-making is usually challenging in the absence of accurate formation information. Processes like well testing and production logging will provide us important reservoir properties. However, acquisition of a comprehensive data set, in general, is a costly luxury that is not financially feasible for all investment budget ranges (Maysami, 2013). In reality, a significant portion of wells is controlled to produce at a low bottom hole pressure from the beginning of the development (the Strategy 1 introduced in Section 1.2). This indiscriminate strategy might yield a relatively safe NPV if we are lucky. However, for mosf the time, the naïve well control will undermine the productivity potential of the reservoir. An economic decision-making method is badly in need.

A data-driven algorithm is proposed which establishes a direct link between the next step production plan and the wellhead response. Compared with Strategy 1, the data-driven solution (Strategy 3) leads to up to 15% increase on 5-year NPV. The Strategy 3 is negligibly inferior to the Strategy 2 that generated by optimization program regarding NPV.

The data-driven algorithm was applied on the numerical simulation model introduced in Chapter 2, and the results were compared with Strategy 1 and Strategy 2. Given an arbitrary parameter setting, the algorithm worked perfectly for cases with concave fractional flow curves. For cases with ‘S-shape’ fractional flow, the final NPV given by

Strategy 1 and Strategy 2 have no distinct difference. In this case, the algorithm guarantees a solution that is at least as good as Strategy 1.

4.1 Data-Driven Algorithm Description

For simplicity, reservoirs with concave shape fractional flow curves (*ng = 0.5* and *ng = 1* cases) are defined as type A reservoirs and reservoirs with S-shape fractional flow curves (*ng = 2* and *ng = 4* cases) are entitled type B reservoirs.

As was concluded in Chapter 3, production strategy of type B reservoirs has little room to improve. The Strategy 1 is already sufficient to yield a desirable NPV. In contrast, for type A reservoirs, a sharp pressure drop at the initial stage of reservoir development would undermine the productivity. A slower pressure drawdown or a pressure hold would initiate an oil saturation build-up and subsequently increase the proportion of oil flow to the surface. However, only pressure hold is applied in the data-driven algorithm because the slow pressure drawdown would be hard to control and output unclear OGR response.

A combination of the conclusions of Chapter 2 and Chapter 3 implies that the OGR response from wellhead is a perfect indicator of the reservoir condition and potential productivity. A critical insight the surface OGR provides is that type B reservoirs can be distinguished from type A reservoirs through a pressure drop test below the bubble point pressure because type B reservoirs will respond a positive OGR while type A reservoirs will give an OGR response that is greater than zero (Figure 2.5). The second information the OGR would offer is the derivative of underground oil flow fraction towards the saturation. When the pressure holds, a strong positive OGR response implies that the reservoir saturation is within a strong response region (Figure 3.2 and Figure 3.4). Keeping

holding the BHP at this period of time will contribute to the final NPV. Conversely, when a near-zero OGR response is obtained, maintaining pressure becomes meaningless, and the best strategy is to drop the pressure as fast as possible and as soon as possible.

The first part the algorithm is to screen type B reservoirs and directly apply Strategy 1 on them. It is easy to accomplish by observing the OGR response the moment when P_b is reached. Such a moment is indicated by a sudden build up or drop in value of the surface OGR. If the OGR builds, the reservoir should be classified as type B. Otherwise, the reservoir is type A. The challenge of the algorithm lies in the second part. While the pressure hold would provide us significant reservoir information and benefit the long-term NPV to some extent, it is typically associated with high risk. The pressure is kept at the expense of the productivity if the drawdown is not yet large enough. Therefore, the decisions on the timing and duration for pressure hold are tricky to make. To improve the economic benefits as much as possible and lower the risk at the same time, a well control strategy is designed that separates the production lifetime into multiple time slices. Within each time slice, the bottom hole pressure is constrained to drop first and then hold suddenly. The well control of each time slice is defined as a drop hold cycle (DHC). For example, Figure 4.1 shows a 3-DHC control scheme. Each time slice lasts 45 days where the pressure drops for 5 days and then holds for the rest 40 days.

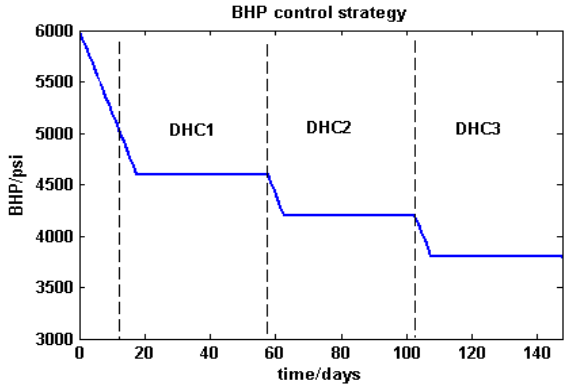

Figure 4.1 Drop-Hold-Cycle Well Control Scheme

Such well control pattern make it possible for decision makers to acquire reservoir information and update development plans every interval of time. It reduces the risk and retrieve reservoir information as much as possible. At the end of each time slice, the OGR response over the hold period is recorded and the average OGR response per day (response rate) is calculated. For the application on a real reservoir, the response rate should be estimated by fitting a linear regression model to the noisy production data. While for the numerical simulation cases, the response rate is simply equal to the OGR difference of last and first day divided by duration of hold period. In this algorithm, the response rate serves as the termination criterion to break the DHC. The DHC will be stopped if the response rate of the last cycle is smaller than a minimum response rate (MRR). BHP will then be dropped with a reduced rate to the lowest allowed to achieve maximum drawdown (Figure 4.2).

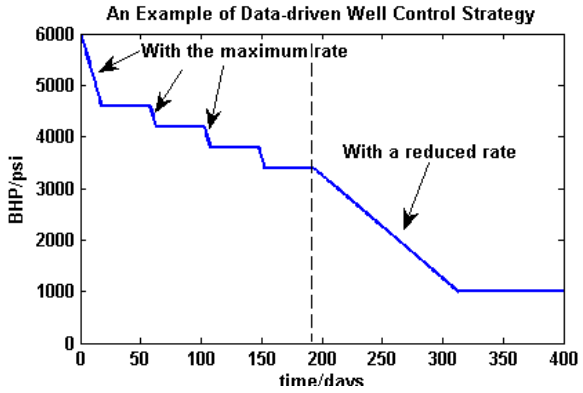

Figure 4.2 An Example of Data-Driven Well Control Strategy

There are four major parameters need to be set for this algorithm: the maximum pressure drop rate (MPDR), the minimum response rate (MRR), the Drop Interval (*d*) and the Hold-Drop-Ratio (*r*). The MRR is the criterion for stopping the DHC. The *d* is the time applied to drop BHP within each DHC. The *r* denotes the ratio between hold time and drop time. MPDR (set to be 80 psi/day in this study) is usually limited by the capability of the bottom hole choke while MRR, *d* and *r* depend on human choice. The choosing of these 3 parameters will be demonstrated in a later section. The pseudo-code of the algorithm is given below.

Data-driven Algorithim

- Drop the pressure to $\boldsymbol{P_b}$ with maximum pressure drop rate (MPDR)
- $\boldsymbol{N_c} = 0$
- Try the first DHC, if $\frac{\partial OGR}{\partial t} > 0$ at the start of the first DHC,
  - Stop doing DHC and return Strategy 1;
- Else,
  - DO
    - DHC
    - N_c++
    - Compute *response rate* for hold period
    - IF (response rate < minimum response rate)
      - Drop BHP to P_{low} with slope MPDR/N_c
      - Break the loop
  - ENDDO
- ENDIF

The algorithm is tested with MPDR = 80 psi/day, d = 5 days, r = 16 and MRR = 1e-4. The BHP control solution carries out four DHCs before the final drop (Figure 4.3 (a)). Figure 4.3 (b) and Figure 4.3 (c) give the variation of OGR and response rate.

The OGR bounds up for each DHC, and it shows a general declining trend. The response rate keeps decreasing for each DHC and the last hold returns a response rate that is smaller than the minimum MRR. The algorithm is terminated at $N_c = 4$ and the BHP is then dropped to P_{low} with 20 psi/day (MDR/N_c).

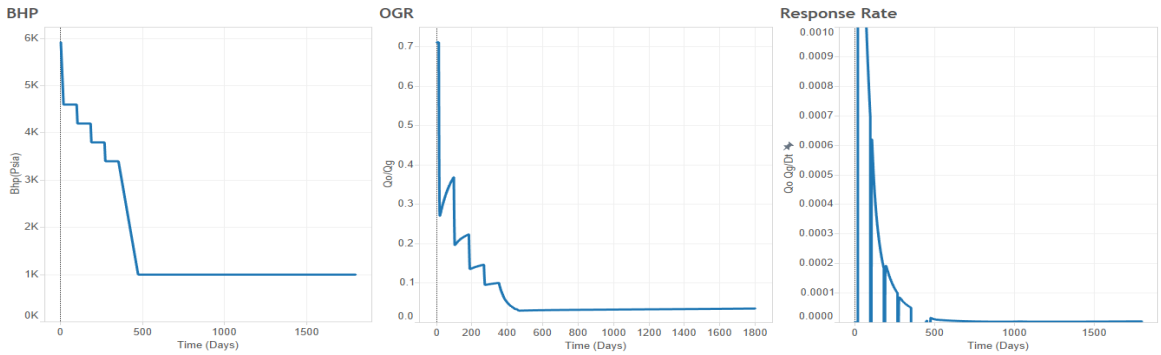

(a) (b) (c)

Figure 4.3 BHP, OGR Response and Response Rate for a Data-Driven Solution

4.2 Basic Solution of the Data-Driven Algorithm

Setting 5 year NPV as the objective function, the BHP control strategies generated by the data-driven algorithm (Strategy 3) are compared with Strategy 1 and Strategy 2. Note NPV in the following case is computed with 45$/bbl oil price, 2.2$/MMBtu gas price and 12% cash depreciation rate.

In all cases, all algorithm parameters are set as follows: MPDR = 80 psi/day; MRR = 1e-4; d = 5 days; r = 16. The NPV versus Time is presented by the following figures, where the yellow curve represents Strategy 1, the red curve denotes Strategy 2 and the blue curve is Strategy 3 results.

ng = 0.5

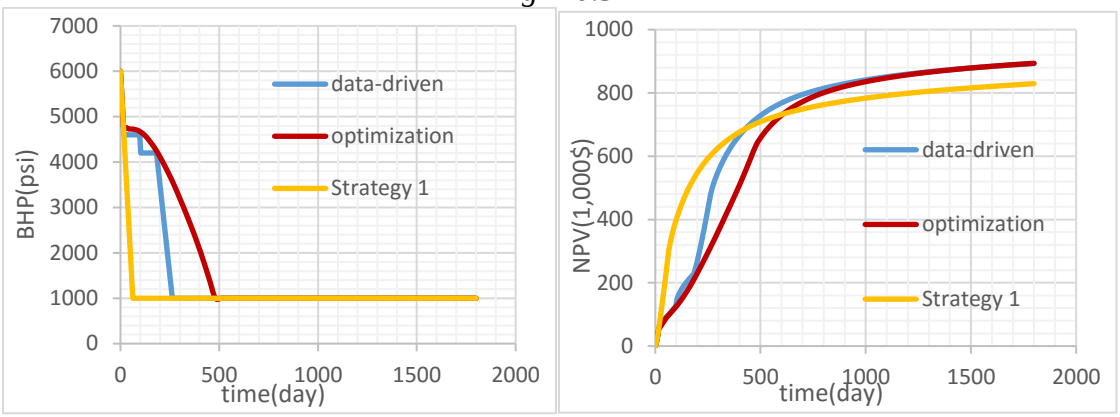

(a) (b)

Figure 4.4 Comparison of Strategy 1, 2, 3 on NPV for *ng = 0.5*

In *ng = 0.5* case, the algorithm run 2 DHC before termination, which indicates that the response rate of the first hold period is strong, but decreased for the second DHC. Following the same mechanisms discussed in Section 3.1.2, it is clear that the saturation dropped into the weak response region when the second DHC was carried out. The performance of the Strategy 3 was as good as optimized well control and they both are much better than the Strategy 1 in terms of 5-year NPV.

ng = 1

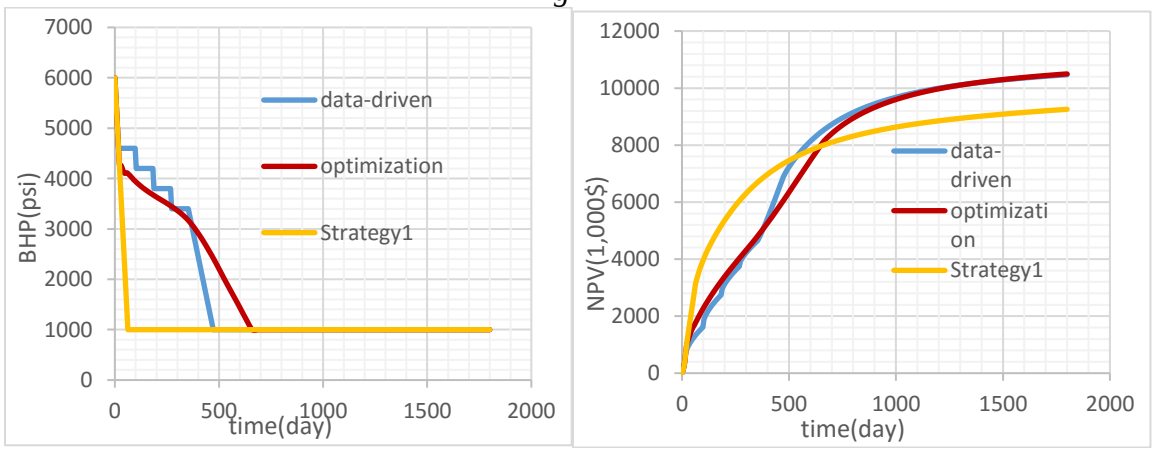

(a) (b)

Figure 4.5 Comparison of Strategy 1, 2, 3 on NPV for *ng = 1*

Four DHCs was run before the algorithm terminated for the *ng=1* case. This is self-explanatory that since the fractional flow curve is less steep, it took more cycles for the

saturation to fall into the weak response part. The Strategy 3 performed comparably to the optimized solution and they both yielded greater NPV prediction than the Strategy 1.

ng = 2

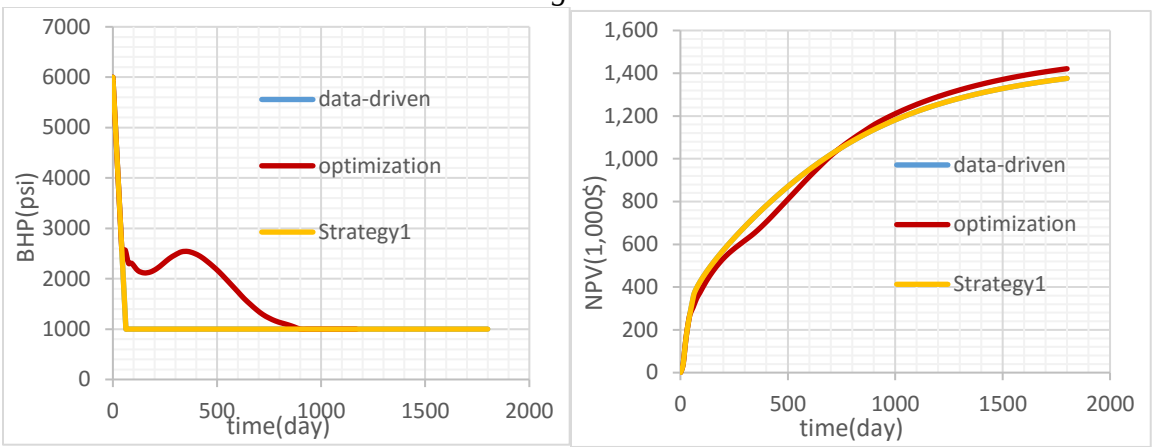

(a) (b)

Figure 4.6 Comparison of Strategy 1, 2, 3 on NPV for *ng = 2*

The Strategy 3 overlapped with the Strategy 1 for both *ng = 2* and *ng = 4* cases (Figure 4.6 (a) and Figure 4.7 (a)) which implies the Strategy 1 is already a satisfactory solution for type B reservoirs. The final NPV of the Strategy 3 is acceptably smaller than the Strategy 2 for *ng = 2* case (Figure 4.6 (b)).

ng = 4

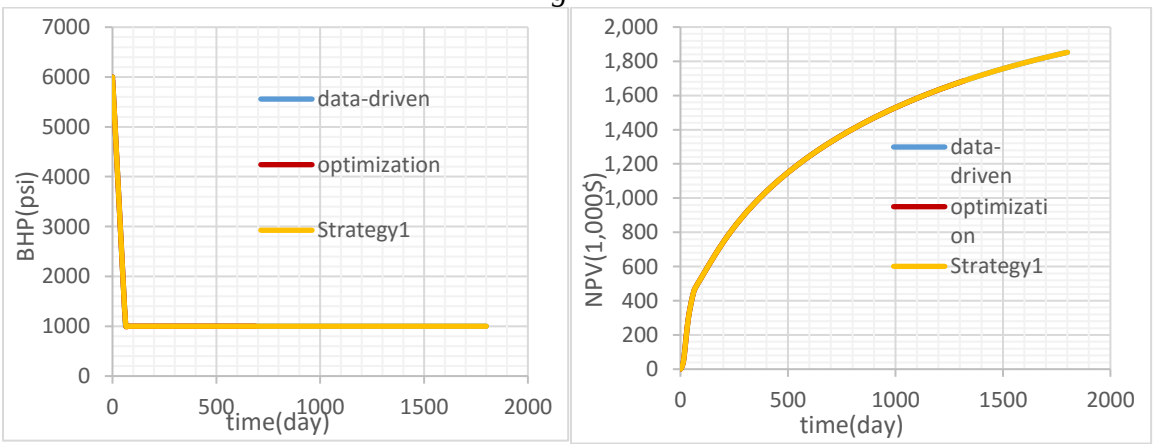

(a) (b)

Figure 4.7 Comparison of Strategy 1, 2, 3 on NPV for *ng = 4*

The data-driven algorithm led to the same well controls as the optimization result for *ng = 4* case. Again, this is because the its fractional flow curve has a very wide weak response region at the rightmost part (Figure 3.8) which yields no space for optimization.

A quick application of the data-driven algorithm on four synthetic reservoirs proved that it is able to offer desirable BHP control plans. The algorithm yielded a naïve well control strategy for type B reservoir which simple and risk-free. The application on type A suggested an active drop-and-hold production control pattern which is near-optimal and easy to apply.

4.3 Discussion on Parameter Setting

As shown in the last section, the data-driven algorithm led to suitable production plans for all cases. Type B reservoirs could benefit from the scheme with no further concerns because the Strategy 1, in this scenario, is already an optimal or near-optimal solution. As long as the asset can be categorized as type B through dropping test below the bubble point, the improved well control is determined instantaneously. However, the application on type A reservoir still needs more work to select the parameters which were discussed in Section 4.1. The following discussion on parameter choice is only for the non-naïve solution of the algorithm.

4.3.1 Choice of Hold-Drop-Ratio (r)

Though rigorously the pressure is not dropped steadily, the DHCs can be considered a BHP drop with a constant rate. In essence, the value of hold-drop-ratio determines the 'average drop rate' of the DHC period. A larger r indicates a smaller average drop rate since more proportion of time is applied to hold the pressure, and it can be risky because longer hold time wastes the opportunity to increase drawdown for better productivity.

In this section, a sensitivity analysis on r is carried out on type A reservoirs of various fluid properties. The drop interval (d) was set to be 5 days, r took the value of 4, 16 and 32 to make comparisons. As the drop interval is constant, bigger r means longer holding time. Different settings of r are compared in the figures below in which the blues represent r = 4 (pressure holding time equals to 20 days), the red denotes r = 16 (holding

time equals to 80 days) and the yellow line stands for r = 32 (holding time equals to 160 days).

ng = 0.5

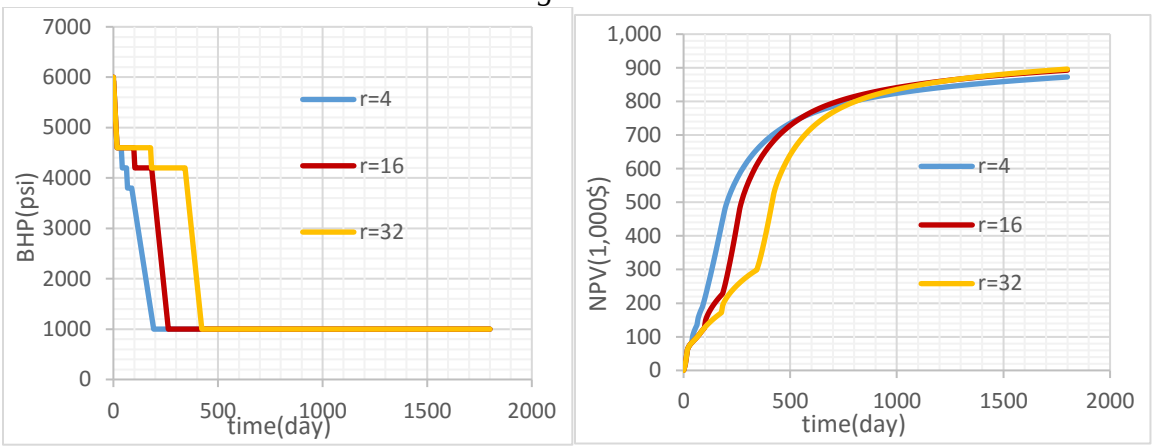

(a) (b)

Figure 4.8 Sensitivity Analysis on Hold-Drop-Ratio for *ng* = 0.5 Case

The larger hold-drop ratio yielded a better strategy for the *ng* = 0.5 case. The cases of r = 16 and r = 32 generated comparable NPV predictions and were both better than the r = 4 solution. The r = 16 solution is conservative because it tends to return more cash flow at the beginning stage.

ng = 1

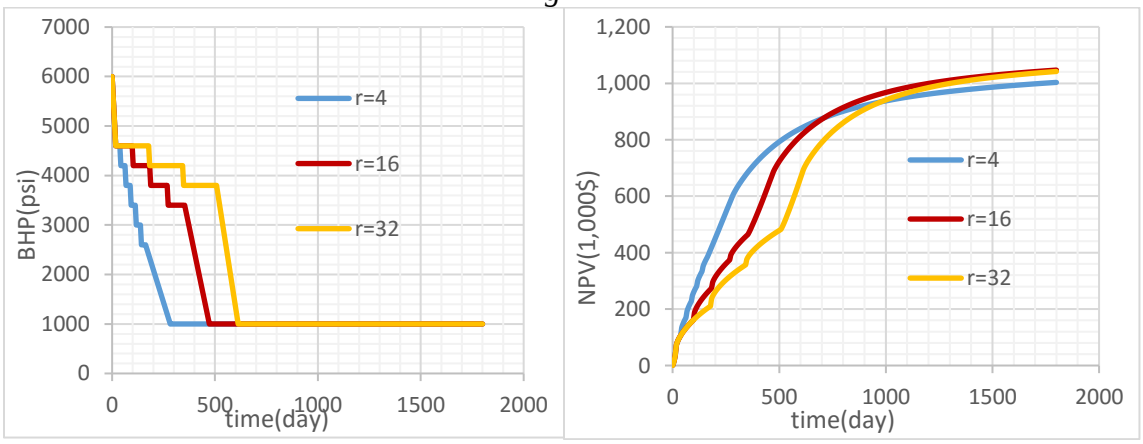

(a) (b)

Figure 4.9 Sensitivity Analysis on Hold-Drop-Ratio for *ng* = 1 Case

The r = 16 led to the best solution for ng = 1 case. Similar with the ng = 0.5 case, the r = 4 predicts less NPV than the other 2 cases.

The choice of r is essentially the tread off between performance and risk. A larger hold-drop-ratio makes longer hold which benefits long term interests for a reservoir with strong OGR response. On the other hand, a small hold-drop-ratio weighs more on the effect of a significant drawdown to improve productivity.

4.3.2 Choice of Drop Interval (d)

Another test is made to the analyze the selection of drop interval (d). The d determines the duration of each DHC which in turn reflects the frequency that the decision makers retrieve reservoir information through the OGR response. A small drop interval updates information more frequently and takes shorter interval to make new decisions. Theoretically, the smaller drop interval is better because more details is provided for decision-making. But, in reality, small drop interval may yield unclear OGR response because the influence of the last DHC's pressure wave needs time to fade out.

ng = 0.5

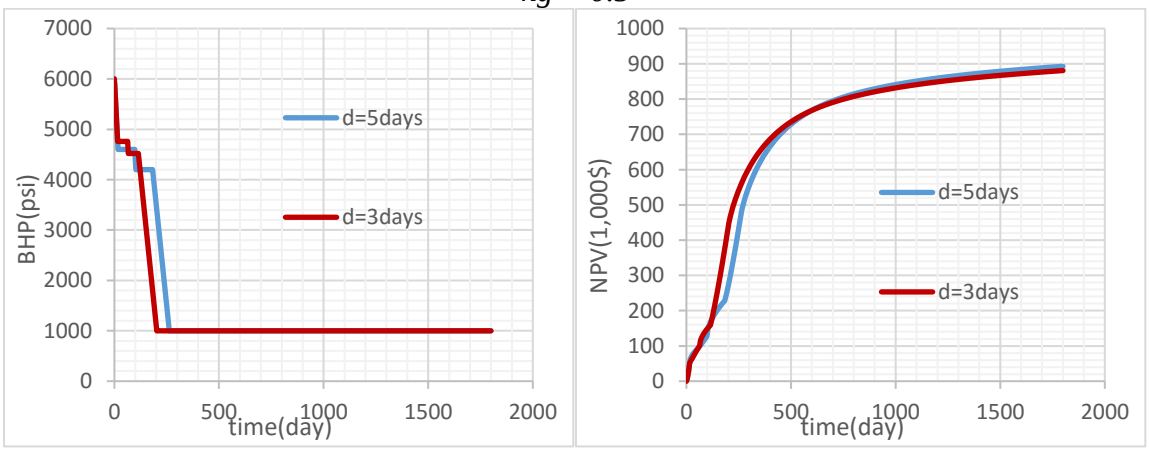

(a) (b)

Figure 4.10 Sensitivity Analysis on Drop Interval for ng = 2 Case

In this section, hold-drop-ratio was set to be 16; *d* took the value of 3, and 5 to make a comparison. Figure 4.10 and Figure 4.11 give the improved strategies of *ng = 0.5* and *ng = 1* respectively. For two different drop interval values, the well controls were carried out in the same manner: First, the 'average drop rate' of DHCs are the same as long as the hold-drop-ratios are equal; Second, the DHC terminated at a similar time. Consequently, NPV vs time curves of both cases are almost the same.

ng = 1

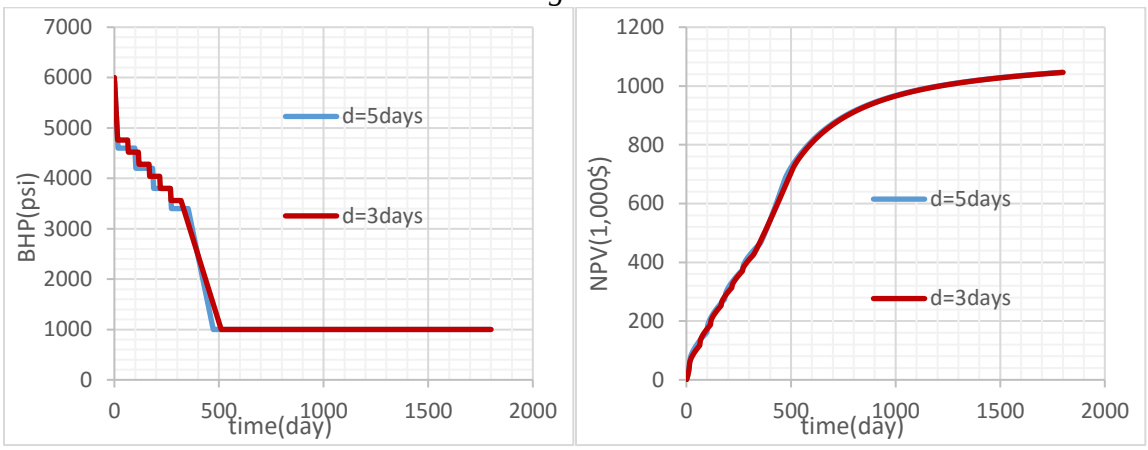

(a) (b)

Figure 4.11 Sensitivity Analysis on Drop Interval for *ng* = 1 Case

An important aspect is that different parameter setting for the algorithm did not make very big difference regarding final NPVs. (Figure 4.8-Figure 4.11). This implies that the algorithm performance is quite stable, and few efforts are required to take on the parameter selection. For all cases we have tested, parameter setting in Section 4.2 (*r* = 16 and *d* = 5) is a desirable choice.

CHAPTER 5

SUMMARY, CONCLUSIONS AND RECOMMENDATIONS

5.1 Summary and Conclusions

The thesis has three main parts. 1, the introduction of a well control generating algorithm as well as a discussion on its parameter selection, 2, the verification of the algorithm's performance through comparisons with model-based optimization results, and 3, the illustration of the underlying physics behind the proposed method.

Based on the study of this thesis, the following conclusions were made:

1. For unconventional reservoirs developed with multi-stage fractured wells, the relationship between the BHP and oil saturation of the hydraulic fracture can be described as: (1) When the BHP drops below P_b, the oil saturation decreases simultaneously with the pressure. (2) When the BHP is kept constant after a dramatic drawdown, the saturation within hydraulic fracture, as well as its proximity, will build up as the gas phase move backward into the reservoir.
2. The wellhead OGR response is a combination of both pressure and saturation contributions. When the BHP drops and the oil flow fraction is sensitive to the saturation, the contribution of saturation will dominate. Otherwise, pressure contribution will overwhelm. When the BHP is maintained, and subsequently saturation builds up, a positive OGR response is expected, and the intensity of the OGR response is determined by the

fractional flow property. The OGR response, in turn, provides significant information about the reservoir fluid and is able to assist production decision-making

3. The optimization results indicate that type A reservoir would benefit from slowing down pressure drop and type B reservoirs have limited room for improvement.
4. The proposed data-driven algorithm is capable of increasing the five-year NPV for type A reservoirs by up to 15% and guaranteeing a near-optimal solution for type B reservoirs The method is characterized by low risk and could be served as complementary for the model-based optimization.

5.2 Recommendations

The method introduced in the thesis offers a great possibility to improve the production plan for fractured unconventional reservoir developed by natural energy at the beginning stage. However, the uncertainty and complexity inherent in the field data would hinder the application of the algorithm on real reservoirs. A significant difference between the output of a real reservoir and a simulation model is that the real history data can be very noisy while the simulation data is associated with less fluctuation. The history data is typically biased because of the dynamic interaction between the fluid flow and wellbore and the presence of measurement error while the simulation always reflects the true response of the numerical reservoir model. The measurement error, to some extent, could be addressed by applying a statistical scheme. The influence of wellbore (e.g. wellbore

storage effect), however, requires more efforts on the establishment of a mature wellbore model.

A detailed procedure for practical application of the algorithm is listed below.

1. Start to drop the BHP with the maximum rate; Keep dropping the pressure until a lasting change on OGR is observed (Try to distinguish a significant change from common variation); The change indicates that the bubble point pressure is reached;
2. If the OGR increases, carry out Strategy 1 and the algorithm is over, otherwise,
3. Start DHCs: record OGR data and bootstrap multiple ensembles of the OGR data (explained by Figure 5.1 and Figure 5.2); make sure the data is collected as (*t*, OGR) pairs; Fit lines for each ensemble and treat the slope of each line as the samples of response rate;
4. Compute the 95% confidence interval for the response rate; If the lower bound of the interval is greater than the minimum response rate, return to step 3 and keep doing DHC. Otherwise, terminate the DHCs and drop pressure with a reduced rate.

The performance and risk trade-off could be manipulated by applying different confidence interval. Field tests remain to be done to select a desirable confidence level.

A example is given for step 3 to illustrate how to the bootstrap works. For simplicity, it was assumed that ten pairs of (*t*,OGR) data was obeserved during the hold period of a DHC. Figure 5.1 shows a linear model fitted by the full data set. Four ensembles were generated through ramdon sampling and linear models were trained by the four set of data.

The fitted models are demonstrated in Figure 5.2 in which drak blue respresents the sampled data and light blue is the unselected data. The sampling process should be done with replacement. The ensenble data size was set to be 7. However, only 5 data points are displayed on each plots of Figure 5.2 because two data points have been sampled twice.

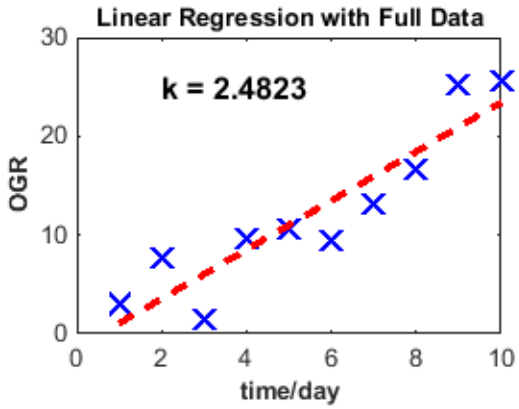

Figure 5.1 Linear Regression with Full Data

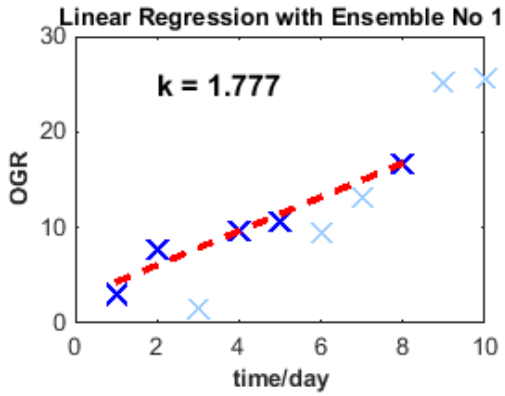

(a) Ensemble No.1

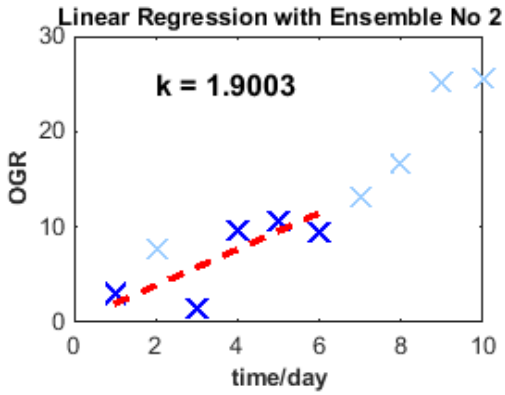

(b) Ensemble No.2

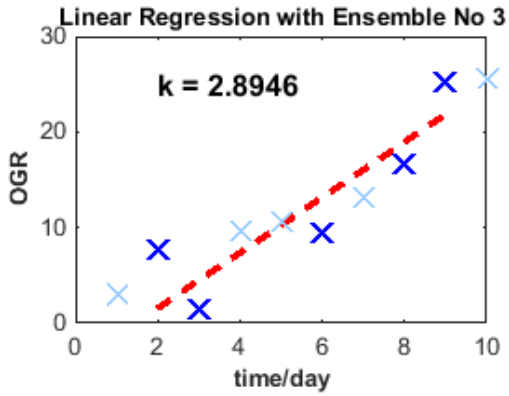

(c) Ensemble No.3

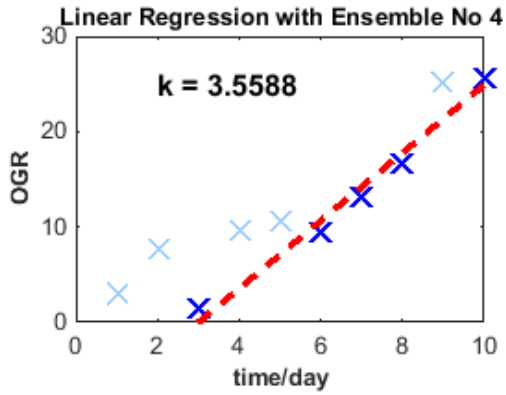

(d) Ensemble No.4

Figure 5.2 Linear Regression with Sampled Data

SYMBOLS

α_k	Line search step size	
C_p	The contribution rate of pressure to OGR response	/psi
C_s	The contribution rate of saturation to OGR response	/psi
d	Time used to drop BHP for each DHC	day
d_k	Search direction for *k*th step	
E	Minimum response rate	/day
f_o	Oil flow fraction	
H	Time used to hold BHP	day
k_{fr}	Fracture permeability	md
k_{rg}	Relative gas permeability	md
$K_{rg,max}$	Maximum gas saturation	md
k_{ro}	Relative oil permeability	md
$K_{ro,max}$	Maximum oil saturation	md
N_c	Number of drop-hold cycle	
N_e	Ensemble Size	
n_g	Gas exponent in Corey model	
n_o	Oil exponent in Corey model	

P_b	Bubble point pressure	psi
P_{low}	Lowest BHP allowed	psi
P_i	Initial reservoir pressure	psi
r	hold-drop-ratio	
R_s	Solution gas oil ratio	mcf/stb
S_{gc}	Critical gas Saturation	
S_{or}	Residual oil Saturation	
$\tilde{x}_i$	Scaled Variables	
x^k	Independent Variables for kth step	
μ_g	Gas viscosity	cp
μ_o	Oil viscosity	cp

ABBREVIATIONS AND CONCEPT DEFINITIONS

Abbreviations

DHC	BHP **D**rop **H**old **C**ycle
GOR	Production **G**as **O**il **R**atio
MPDR	**M**aximum **P**ressure **D**rop **R**ate
MRR	**M**inimum **R**esponse **R**ate
NPV	**N**et **P**resent **V**alue
OGR	Production **O**il **G**as **R**atio, equal to 1/GOR

Concept Definition

Contribution Rate	Influence on the OGR per unit pressure or saturation change
Drop Interval (*d*)	Time used to drop BHP within each DHC
Hold Interval (*h*)	Time used to hold BHP within each DHC
Hold-Drop-Ratio (*r*)	Hold interval / Drop interval
Response Rate	OGR response / Hold interval
Strategy one	The well control strategy that drop BHP to Plow and keep to end
OGR Response	Change of OGR within a certain Hold Interval

BIBLIOGRAPHY

Bhattacharya, S. M. (2014). Causal analysis and data mining of well stimulation data using classification and regression tree with enhancements. *Mathematics of Planet Earth*, 665-668.

Chen, Y. O. (2009). Efficient ensemble-based closed-loop production optimization. *SPE Journal*, 14(04), 634-645.

Corey, A. T. (1954). The interrelation between gas and oil relative permeabilities. *Producers monthly*, 19(1): 38-41.

Dake, L. P. (1983). *Fundamentals of Reservoir Engineering.* Elsevier.

Forouzanfar, F. (2012). *Well-placement Optimization* (Doctoral dissertation). THE UNIVERSITY OF TULSA.

Gupta, S. F. (2014). Production forecasting in unconventional resources using data mining and time series analysis. *SPE/CSUR Unconventional Resources Conference–Canada.* Society of Petroleum Engineers.

Hastie, T. T. (2001). *The Elements of Statistical Learning.* NY: Springer.

Hillis, D. M. (n.d.). An empirical test of bootstrapping as a method for assessing confidence in phylogenetic analysis. *Systematic Biology*, 42(2), 182-192.

Jansen, J. D. (2005). Closed-loop reservoir management. *First Break*, 23(1), 43-48.

Jansen, J. D. (2009). Closed loop reservoir management. *SPE Reservoir Simulation Symposium.* Society of Petroleum Engineers.

Lafollette R, H. W. (2012). Practical data mining: analysis of Barnett shale production results with emphasis on well completion and fracture stimulation. *SPE Hydraulic Fracturing Technology Conference.* Society of Petroleum Engineers.

Maysami, M. G. (2013). Data Driven Analytics in Powder River Basin, WY. *SPE Annual Technical Conference and Exhibition.* Society of Petroleum Engineers.

Oliver D S, R. A. (2008). *Inverse theory for petroleum reservoir characterization and history matching.* Cambridge University Press.

Parashar M, K. H. (2005). Application of grid-enabled technologies for solving optimization problems in data-driven reservoir studies. *Future Generation Computer Systems*, 21(1), 19-26.

Schuetter, J. M. (2015). Data Analytics for Production Optimization in Unconventional Reservoirs. *Unconventional Resources Technology Conference.* Society of Petroleum Engineers.

Yeten, B. B. (2004). Decision analysis under uncertainty for smart well deployment. *Journal of Petroleum Science and Engineering*, 44(1), 175-191.

Younis R M, A. K. (2011). *Modern advances in software and solution algorithms for reservoir simulation* (Doctoral dissertation). Stanford University.

APPENDIX A

RESERVOIR PARAMETERS FOR THE SIMULATION MODEL

Table 6.1 Basic Reservoir Parameter

Reservoir Parameters			
grid dimension	1720	23	1
reservoir dimension	2000 ft	300 ft	200 ft
porosity	0.03		
X permeability	100 nd		
Y permeability	100 nd		
Z permeability	30		
Density(Oil, Water, Gas)	49.1	64.79	0.06054
ROCK compressibility	3.00E-06		
Bubble point pressure(Pb)	5000 psi		
Initial reservoir pressure(at mid deep)	6000 psi		
Fracture Parameters			
single fracture dimension	0.01 ft	hf 150ft	200ft
porosity of fracture	1		
X permeability of fracture	1000 md		
Y permeability of fracture	1000 md		
Z permeability of fracture	1000 md		
configuration	10stages, 40 fractures		
Well Parameters			
well diameter	0.4 ft		
number of fractures intersect	40		

Table 6.2 Oil PVT

Rs (cf/std)	Rs (mcf/std)	P (psi)	Bo (rb/std)	μ (cp)
140	0.14	800	1.2	1.09
180	0.18	1000	1.225	1.01
220	0.22	1200	1.24	0.96
260	0.26	1400	1.28	0.9
300	0.3	1600	1.285	0.85
350	0.35	1800	1.31	0.77
400	0.4	2000	1.335	0.74
450	0.45	2200	1.36	0.70
500	0.5	2400	1.385	0.66
550	0.55	2600	1.41	0.62
600	0.6	2800	1.43	0.58
650	0.65	3000	1.46	0.54
710	0.71	3200	1.485	0.51
840	0.84	3600	1.55	0.45
980	0.98	4000	1.62	0.40
1130	1.13	4400	1.675	0.37
1310	1.31	4800	1.73	0.35
1405	1.405	5000	1.76	0.335
1500	1.405	5200	1.75	0.34
1700	1.405	5600	1.74	0.36
1910	1.405	6000	1.73	0.37
2120	1.405	6400	1.71	0.39
2330	1.405	6800	1.7	0.40

Table 6.3 Gas PVT Table

P (psi)	Bg (rb/scf)	µg (cp)	P (psi)	Bg (rb/scf)	µg (cp)
800	4.518264	0.012798	3200	1.030154	0.023541
1000	3.287464	0.013918	3600	0.922554	0.025141
1200	2.90367	0.014908	4000	0.814954	0.026741
1400	2.58707	0.015888	4400	0.748581	0.02838
1600	2.27047	0.016868	4800	0.683781	0.03002
1800	1.95387	0.017848	5000	0.651381	0.03084
2000	1.63727	0.018828	5200	0.636817	0.031646
2200	1.495408	0.019604	5600	0.610517	0.033256
2400	1.367408	0.020364	6000	0.584217	0.034866
2600	1.257492	0.021141	6400	0.557917	0.036476
2800	1.171892	0.021941	6800	0.531617	0.038086
3000	1.086292	0.022741			